
Raytheon

# SNOW COVER/DEPTH

## VISIBLE/INFRARED IMAGER/RADIOMETER SUITE ALGORITHM THEORETICAL BASIS DOCUMENT

**Version 3: May, 2000**

Ken Jensen
Igor Appel

*Science Team Members:*
*Dr. Knut Stamnes, Stevens Institute of Technology*
*Dr. William Emery, University of Colorado*

RAYTHEON SYSTEMS COMPANY
Information Technology and Scientific Services
4400 Forbes Boulevard
Lanham, MD 20706

SRBS Document # Y2401

EDR: SNOW COVER / DEPTH

Doc No: Y2401

Version: 3

Revision: 0

| | Function | Name | Signature | Date |
|---|---|---|---|---|
| Prepared by | EDR Developer | K. JENSEN | | |
| Approved by | Relevant IPT Lead | K. JENSEN | | |
| Approved by | Chief Scientist | P. ARDANUY | | |
| Released by | Program Manager | H. BLOOM | | |

# TABLE OF CONTENTS

Page

LIST OF FIGURES ..... iii

LIST OF TABLES ..... v

GLOSSARY OF ACRONYMS ..... vi

ABSTRACT ..... ix

1.0 INTRODUCTION ..... 1
- 1.1 PURPOSE ..... 1
- 1.2 SCOPE ..... 1
- 1.3 VIIRS DOCUMENTS ..... 1
- 1.4 REVISIONS ..... 2

2.0 EXPERIMENT OVERVIEW ..... 3
- 2.1 OBJECTIVES OF THE SNOW COVER RETRIEVAL ..... 3
- 2.2 INSTRUMENT CHARACTERISTICS ..... 5
- 2.3 RETRIEVAL STRATEGY ..... 7
  - 2.3.1 Snow Binary Map ..... 7
  - 2.3.2 Snow Fraction ..... 8

3.0 ALGORITHM DESCRIPTION ..... 9
- 3.1 PROCESSING OUTLINE ..... 9
- 3.2 ALGORITHM INPUT ..... 9
  - 3.2.1 VIIRS Data ..... 9
    - 3.2.1.1 Instrument Quality ..... 9
    - 3.2.1.2 Geolocation ..... 10
    - 3.2.1.3 Solar / Sensor Geometry ..... 10
    - 3.2.1.4 Surface Reflectance ..... 10
    - 3.2.1.5 Cloud Mask ..... 10
    - 3.2.1.6 Land/Water Mask ..... 10
    - 3.2.1.7 Forest Mask ..... 10
    - 3.2.1.8 Non-Snow Reflectance Spectra ..... 11
    - 3.2.1.9 Snow Reflectance Spectra ..... 11
  - 3.2.2 Non-VIIRS Data ..... 11
- 3.3 THEORETICAL DESCRIPTION OF THE RETRIEVAL ..... 11
  - 3.3.1 Physics of the Problem ..... 11

3.3.2 Mathematical Description of the Snow Binary Map Algorithm ..... 14
3.3.3 Mathematical Description of the Snow Fraction Algorithm ..... 17
3.3.3.1 Endmember Selection (Non-Snow Reflectance) ..... 18
3.3.3.2 Snow Reflectance ..... 19
3.3.4 Archived Algorithm Output ..... 19

4.0 EDR PERFORMANCE ..... 20
4.1 STRATIFICATION ..... 20
4.1.1. Snow Binary Map ..... 20
4.1.2 Snow Fraction ..... 21
4.2 STRATIFIED PERFORMANCE ANALYSIS ..... 21
4.2.1. Snow Binary Map ..... 21
4.2.2 Snow Fraction ..... 35
4.3 LIMITS OF APPLICABILITY ..... 38
4.3.1 Cloudy ..... 38
4.3.2 Low Light or Nighttime ..... 39
4.3.3 Forest canopy (snow fraction) ..... 39
4.4 PRACTICAL CONSIDERATIONS ..... 39
4.4.1 Numerical Computation Considerations ..... 39
4.4.2 Programming and Procedural Considerations ..... 39
4.4.3 Configuration of Retrievals ..... 39
4.4.4 Quality Assessment and Diagnostics ..... 40
4.4.5 Exception Handling ..... 40

5.0 INITIALIZATION AND VALIDATION ..... 42
5.1 INITIALIZATION ..... 42
5.2 PRE-LAUNCH CHARACTERIZATION ..... 43
5.3 VALIDATION ..... 43

6.0 ASSUMPTIONS ..... 44

7.0 REFERENCES ..... 46

# LIST OF FIGURES

Page

Figure 1. Expected signal-to-noise performance for the three VIIRS fine resolution bands used in the binary snow map algorithm. 5

Figure 2. Expected signal-to-noise performance for the three VIIRS fine resolution bands and 7 VIIRS moderate resolution bands used in the snow fraction algorithm. 7

Figure 3. Representative reflectance spectra for snow, vegetation, soil, and water (from Klein, Hall, and Riggs, 1998). 13

Figure 4. Representative reflectance spectra for snow and clouds (from Hall et al., 1998). 13

Figure 5. Near-Infrared Reflectance versus NDSI plot for winter and summer Landsat TM scenes of Glacier National Park, Montana (from Hall et al., 1998). Pixels located in the cross-hatched region are classified as snow. Winter forest pixels, which are known to have snow cover under the forest canopy, are incorrectly classified as no snow. 15

Figure 6. NDSI versus NDVI plot for modeled aspen, jack pine, and spruce stands (from Klein, Hall, and Riggs, 1998). The hatched region is the snow classification region for the Version 4 MODIS algorithm. The gray shaded region represents a proposed additional region for capturing snow-covered forests. 16

Figure 7. (a) Visible reflectance image of Death Valley scene from MAS/SUCCESS campaign. The grey-scale is from 0.0 to 0.5 in reflectance. (b) Short Wave IR reflectance image of the scene. The grey-scale is from 0.0 to 0.5 in reflectance. 23

Figure 8. NDSI versus NDVI scatter plot of the MAS Death Valley scene (SUCCESS_115_16). The image has been aggregated to a VIIRS pixel size at nadir. 24

Figure 9: (a) Visible reflectance image of Brazil scene from MAS/SCAR-B campaign. The color scale is from 0.0 to 0.2 in reflectance. (b) NDVI image of the scene. The color scale is from 0.05 to 0.7 in NDVI units. (c) NDSI image of the scene. The color scale is from –0.5 to 0.07 in NDSI units. 25

Figure 10. NDSI versus NDVI scatter plot of the MAS Brazil scene (SCAR-B_163_1). The image has been aggregated to a VIIRS pixel size at nadir. 26

Figure 11. (a)Visible reflectance image of Minnesota winter scene from MAS/WINCE campaign. The grey-scale is from 0.0 to 1.0 in reflectance. (b) Normalized Difference Snow Index (NDSI) image of the scene. The color scale is from NDSI = 0.0 (darkest) to NDSI = 0.8. (c) Normalized Difference Vegetation Index (NDVI) image of the scene. The color scale is reversed, from NDVI = 0.25 (darkest) to NDVI = 0.05. 27

Figure 12. NDSI versus NDVI scatter plot of the MAS Minnesota winter scene (WINCE_49_06). The image has been aggregated to a VIIRS pixel size at nadir..... 28

Figure 13. (a) Visible Reflectance at 50 meter resolution, taken from a 0.648 micron image of Eastern Colorado obtained by the MODIS Airborne Simulator (MAS) on February 13, 1997. The extent of the scene is 35 km x 100 km. (b) Snow fraction at 0.4 km resolution, obtained by classification and aggregation to a VIIRS pixel size at nadir. (c) Retrieved Binary Snow Cover map. System performance errors were used to simulate a VIIRS retrieval. Green cells are mapped as snow. 97.8 % of the pixels were correctly typed. ..... 29

Figure 14. NDSI versus NDVI scatter plot of the MAS Colorado winter scene (WINCE_50_14). The image has been aggregated to a VIIRS pixel size at nadir..... 30

Figure 15. NDSI versus NDVI scatter plot the MAS Colorado winter scene (WINCE_50_14). The image has been aggregated to a VIIRS pixel size at nadir. Error perturbations have been added to the scene..... 31

Figure 16. Probability of Correct Typing vs. Snow Fraction for the MAS Colorado winter scene (WINCE_50_14). The scene was aggregated to a pixel size of 0.4 km to simulate a VIIRS nadir view. ..... 32

# LIST OF TABLES

Page

Table 1. Specifications of the VIIRS Snow Cover/Depth (Binary Map) EDR ..... 3

Table 2. Specifications of the VIIRS Snow Cover/Depth (Snow Fraction) EDR ..... 4

Table 3. Snow Binary Map Algorithm – Input Data Summary ..... 5

Table 4. Snow Fraction Algorithm – Input Data Summary ..... 6

Table 5. VIIRS Data for the VIIRS Snow Cover Algorithms ..... 9

Table 6. Snow Binary Map : Probability of Correct Typing (%) Clear, Nadir, SZA = 60 degrees, Some Canopy, Mixed Snow/No Snow ..... 32

Table 7. Error Budget for Retrieval of the Snow Binary Map EDR ..... 33

Table 8. Error Budget for Retrieval of the Snow Binary Map EDR ..... 34

Table 9. Error Budget for Retrieval of the Snow Binary Map EDR ..... 34

Table 10. Snow Fraction Measurement Uncertainty: Clear, 10% Mixed Pixels (Easy case) ..... 37

Table 11. Snow Fraction Measurement Uncertainty: Clear, 30% Mixed Pixels (Typical case) ..... 37

Table 12. Snow Fraction Measurement Uncertainty : Clear, 50% Mixed Pixels (Hard Case) ..... 37

Table 13. Error Budget for Retrieval of the Snow Fraction EDR ..... 38

# GLOSSARY OF ACRONYMS

| | |
|---|---|
| AMSR | Advance Microwave Scanning Radiometer |
| AOT | Aerosol Optical Thickness |
| ATBD | Algorithm Theoretical Basis Document |
| AVIRIS | Airborne Visible/Infrared Imaging Spectrometer |
| BRDF | Bidirectional Reflectance Distribution Function |
| CMIS | Conical Scanning Microwave Imager/Sounder |
| DAAC | Distributed Active Archive Center |
| EDC | EROS Data Center |
| EDR | Environmental Data Record |
| ENVI | Environment for Visualizing Images |
| GCM | General Circulation Model |
| GIFOV | Ground Imaged Field of View |
| GLI | Global Imager |
| GSD | Ground Sampled Distance |
| HCS | Horizontal Cell Size |
| IP | Intermediate Product |
| LUT | Look-Up Table |
| MAS | MODIS Airborne Simulator |
| MESMA | Multiple Endmember Spectral Mixture Analysis |
| MODIS | Moderate Resolution Imaging Spectroradiometer |
| MTF | Modulation Transfer Function |
| NDSI | Normalized Difference Snow Index |
| NDVI | Normalized Difference Vegetation Index |
| NIR | Near Infrared |
| NOAA | National Oceanographic and Atmospheric Administration |
| NPOESS | National Polar-orbiting Operational Environmental Satellite System |
| NPP | NPOESS Preparatory Program |
| PDR | Preliminary Design Review |
| RDR | Raw Data Record |
| RMS | Root Mean Square |
| SCAR-B | Smoke, Clouds, and Radiation - Brazil |
| SDR | Sensor Data Record |
| SMA | Spectral Mixture Analysis |
| SRD | Sensor Requirements Document |
| SSM/I | Special Sensor Microwave/Imager |
| SUCCESS | Subsonic Aircraft Contrail and Cloud Effects Special Study |
| SWE | Snow-Water Equivalence |
| SWIR | Short Wave Infrared |

| | |
|---|---|
| SZA | Solar Zenith Angle |
| TBD | To Be Determined |
| TBR | To Be Reviewed |
| TM | Thematic Mapper |
| TOA | Top-of-Atmosphere |
| VIIRS | Visible/Infrared Imager/Radiometer Suite |
| VIS/IR | Visible/Infrared |
| WINCE | Winter Cloud Experiment |

# ABSTRACT

The following document is version 3 of the Algorithm Theoretical Basis Document (ATBD) for Snow Cover/Depth retrieval from surface reflectances. The reflectances are to be derived from Top-of-Atmosphere radiances received by the National Polar-orbiting Operational Environmental Satellite System (NPOESS) Visible/Infrared Imager/Radiometer Suite (VIIRS). Snow Cover/Depth, a VIIRS level 2 product, is one of the required VIIRS Environmental Data Records (EDRs) as stated in the VIIRS Sensor Requirements Document (SRD). The surface reflectances will be supplied as a product of the VIIRS Albedo EDR, as documented in the VIIRS Atmospheric Correction over Land ATBD (Y2411). The purpose of this document is to describe the theoretical basis and development process of the algorithms to retrieve a binary snow/no snow map and the fraction of snow cover in a specified horizontal cell, as required by the VIIRS SRD.

The VIIRS Snow Cover EDR threshold requirement is that a binary snow/no snow map be produced at a horizontal cell size of 0.5 km at nadir under clear, daytime conditions, with a probability of correct typing of 90% or better. The algorithm to retrieve the binary map uses the surface reflectance in three VIIRS fine resolution reflectance bands. It is an adaptation of the MODIS snow algorithm, which classifies a pixel as snow or no snow from its values of Normalized Difference Snow Index (NDSI) and Normalized Difference Vegetation Index (NDVI). The VIIRS algorithm uses a red band in place of the green band used by the MODIS algorithm, allowing us to achieve fine resolution (0.4 km at nadir). Our analysis shows that the red band NDSI threshold is nearly identical to the green band NDSI threshold. Our performance analysis leads to a performance estimate of 95% or better probability of correct typing for most cases, consistent with the expected performance of the MODIS algorithm. The algorithm, which will benefit directly from MODIS heritage, is a low risk approach with the capability of providing an operational, global snow cover product.

The VIIRS Snow Cover EDR objective requirement is that the horizontal extent of snow cover be retrieved globally at a horizontal cell size of 1.3 km under clear, daytime conditions. The measurement range will be the fraction of snow cover from 0 to 1, with a measurement uncertainty of 0.1. The algorithm to retrieve snow fraction uses the surface reflectance in three VIIRS fine resolution reflectance bands and also in seven VIIRS moderate resolution reflectance bands. The algorithm is an application of Multiple Endmember Spectral Mixture Analysis (MESMA). An objective of any spectral mixture analysis is the definition of subpixel proportions of spectral endmembers that may be related to mappable surface constituents. Spectral mixture analysis “unmixes” the mixed pixel, determining the fractions of each spectral endmember which combine to produce the mixed pixel’s spectral signature. Our approach is to model the signature from each pixel as a combination of two components: a pure snow reflectance spectrum and a modeled non-snow reflectance spectrum. The approach is based on the assumption that the non-snow endmember spectrum for each pixel is sufficiently modeled by a monthly mean non-snow reflectance, acquired from an external database. Our performance analysis indicates that the measurement uncertainty requirement can be achieved, except for scenes with forest canopy.

This document presents the algorithm theoretical basis, the input data requirements, the EDR performance specification and error analysis, conditions under which the specification can not be attained, and the plan for initialization and validation. It is a substantial revision of our version 2 algorithm, which should be considered to be completely superseded by the new version

.

# 1.0 INTRODUCTION

## 1.1 PURPOSE

This Algorithm Theoretical Basis Document (ATBD) explains the mathematical background to derive the Snow Cover Environmental Data Record (EDR). This document also provides an overview of required input data, physical theory, assumptions, limitations, and a performance analysis of the described algorithms. The Snow Cover EDR is obtained from measurements of the National Polar-orbiting, Operational Environmental Satellite System (NPOESS) Visible/Infrared Imager/Radiometer Suite (VIIRS). The one EDR described in this document is part of the NPOESS/VIIRS team software package of 29 EDRs.

## 1.2 SCOPE

This document covers the theoretical basis for the derivation of the Snow Cover EDR, which consists of a binary snow/no snow map and snow fraction in a horizontal cell. The purpose and scope of the document are described in Section 1, while Section 2 provides an overview of the snow cover retrieval objectives. Section 3 describes the algorithm, its input data, the theoretical background, and some practical considerations. Section 4 contains the EDR performance analysis and error budget. Section 5 contains the pre-launch and post-launch plan for verification and validation. Section 6 contains assumptions and limitations.

## 1.3 VIIRS DOCUMENTS

This document contains references to other Raytheon VIIRS documents, which are given in italicized brackets. The VIIRS documents cited in this document are:

*[SS154640-001]* VIIRS System Specification

*[PS154640-101]* VIIRS Sensor Specification

*[Y3261]* RDR to SDR Conversion ATBD

*[Y2411]* Atmospheric Correction Over Land ATBD

*[Y2412]* Cloud Mask ATBD

*[Y2477]* VIIRS Snow/Ice Module Level Software Architecture document

*[Y3258]* Earth Location ATBD

## 1.4 REVISIONS

This is the third version. Changes since version 2 include:

- A new algorithm to retrieve the binary snow/no snow map, which is a new requirement
- Revision of the process flow, to include the new algorithm
- Improvements to the error analysis, with additional tests
- A revised error budget

# 2.0 EXPERIMENT OVERVIEW

## 2.1 OBJECTIVES OF THE SNOW COVER RETRIEVAL

Because of its high albedo, snow is an important factor in determining the radiation balance, with implications for global climate studies (Foster and Chang, 1993). General circulation models (GCM) do not simulate the Arctic climate very well (Bromwich and Tzeng, 1994), indicating the need to improve measurements of the global snow cover. Weekly snow cover maps of the Northern Hemisphere have been produced since 1966 by NOAA (Matson, Roeplewski, and Varnadore, 1986; Matson, 1991). Daily and 8-day composite global maps are an objective of the recently launched NASA MODIS instrument (Hall et al., 1998). Regionally, the measurement of snowpack properties is vital to the prediction of water supply and flood potential (Carroll *et al.*, 1989; Chang *et al.*, 1987). Regional snow products with 1 km resolution are produced by the National Weather Service (Carroll, 1990), and are expected at 500 meter resolution from MODIS. The objective of the VIIRS retrieval is to achieve the performance specifications designed to meet the requirements stated in the VIIRS Sensor Requirements Document (SRD). These are given in Table 1 (Binary map) and Table 2 (Snow fraction).

**Table 1. Specifications of the VIIRS Snow Cover/Depth (Binary Map) EDR**

| Parameter | Thresholds | Objectives | Specification Value |
|---|---|---|---|
| a. Horizontal Cell Size, | | | |
| 1. Clear – daytime (Worst case) | 1.3 km (TBR) | N/A | 0.8 km |
| 2. Clear – daytime (At nadir) | 0.5 km (TBR) | N/A | 0.4 km |
| 3. Cloudy and/or nighttime | 12.5 km | N/A | NPOESS / CMIS Capability |
| b. Horizontal Reporting Interval | (TBD) | N/A | Horizontal Cell Size |
| c. Snow Depth Ranges | > 0 cm (Any Snow Thickness) | N/A | > 0 cm (Any Snow Thickness) |
| d. Horizontal Coverage | Land | N/A | Land |
| e. Vertical Coverage | > 0 cm | N/A | > 0 cm |
| f. Measurement Range | Snow / No snow | N/A | Snow / No snow |
| g. Probability of Correct Typing(Clear – daytime) | 90% (TBR) at (TBS) % confidence level | N/A | 95% |
| h. Mapping Uncertainty, Clear | 3 km | N/A | 0.067 km (nadir) |
| m. Minimum Swath Width | 3000 km (TBR) | N/A | 3000 km |
| Units: Dimensionless | | | |

**Table 2. Specifications of the VIIRS Snow Cover/Depth (Snow Fraction) EDR**

| Parameter | Thresholds | Objectives | Specification Value |
|---|---|---|---|
| a. Horizontal Cell Size, | | | |
| 1. Clear – daytime (Worst case) | 1.3 km (TBR) | 1 km | 1.6 km |
| 2. Clear – daytime (At nadir) | N/A | N/A | 0.8 km |
| 3. Cloudy and/or nighttime | 12.5 km | 1 km | NPOESS / CMIS Capability |
| b. Horizontal Reporting Interval | (TBD) | (TBD) | Horizontal Cell Size |
| c. Snow Depth Ranges | > 0 cm (Any Snow Thickness) | > 0 cm (Any Snow Thickness) | > 0 cm (Any Snow Thickness) |
| d. Horizontal Coverage | Land | Land & Ice | Land |
| e. Vertical Coverage | > 0 cm | > 0 cm | > 0 cm |
| f. Measurement Range | N/A | 0 – 1 | 0 – 1 |
| n. Measurement Uncertainty (Clear – daytime) | N/A | 10% | 0.1 |
| h. Mapping Uncertainty, Clear | 3 km | 1 km | 0.233 km (worst case) |
| m. Minimum Swath Width | 3000 km (TBR) | (TBD) | 3000 km |
| Units: Dimensionless | | | |

The specifications apply under clear, daytime conditions only. Surface properties can not be observed through cloud cover by a VIS/IR sensor.

## 2.2 INSTRUMENT CHARACTERISTICS

The VIIRS sensor has been designed from the NPOESS sensor requirements and the flowdown of EDR requirements. Complete details on the instrument design are provided in the Raytheon VIIRS Sensor Specification Document *[PS154640-101]*.

The binary map algorithm uses surface reflectance in three bands at fine resolution. Table 3 lists the characteristics of these bands.

**Table 3. Snow Binary Map Algorithm – Input Data Summary**

| λ(μm) | Δλ(μm) | GSD (m) at Nadir (Track x Scan) | HCS (m) at Nadir (Track x Scan) | GSD (m) at Edge of Scan (Track x Scan) | HCS (m) at Edge of Scan (Track x Scan) |
|---|---|---|---|---|---|
| 0.645 | 0.050 | 371 x 131 | 371 x 393 | 800 x 800 | 800 x 800 |
| 0.865 | 0.039 | 371 x 131 | 371 x 393 | 800 x 800 | 800 x 800 |
| 1.61 | 0.060 | 371 x 131 | 371 x 392 | 800 x 800 | 800 x 800 |

Each band has a calibration accuracy specification of 2%. The expected band noise performance provides signal-to-noise better than 100 for most cases, as illustrated in Figure 1.

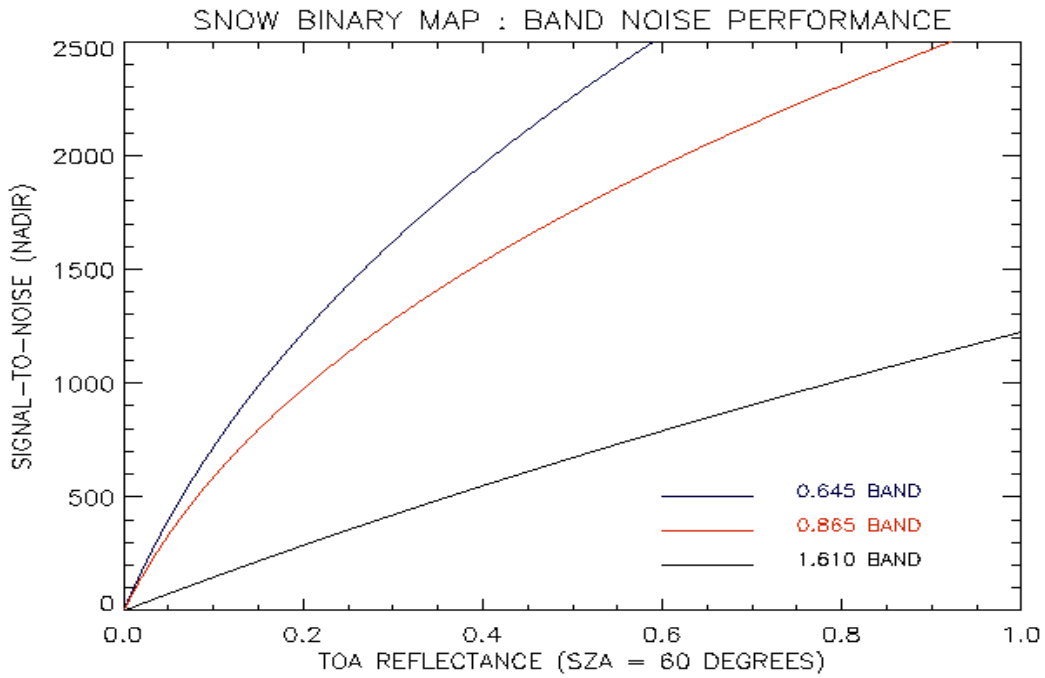


**Figure 1. Expected signal-to-noise performance for the three VIIRS fine resolution bands used in the binary snow map algorithm.**

The snow fraction algorithm uses surface reflectance in 3 bands at fine resolution and 7 bands at moderate resolution. Each is a source of additional information to improve the retrieval. Addition of bands reduces the sensitivity of spectral mixture analysis to accuracy and precision errors in the surface reflectances. Dozier et al. has demonstrated in unpublished work with AVIRIS data that in a linear mixture scenario more bands damp fraction sensitivity to noise and mis-calibration. Table 4 lists the characteristics of the 10 bands used in the snow fraction algorithm.

**Table 4. Snow Fraction Algorithm – Input Data Summary**

| λ(μm) | Δλ(μm) | GSD (m) at Nadir (Track x Scan) | HCS (m) at Nadir (Track x Scan) | GSD (m) at Edge of Scan (Track x Scan) | HCS (m) at Edge of Scan (Track x Scan) |
|---|---|---|---|---|---|
| 0.410 | 0.022 | 742 x 262 | 742 x 786 | 1600 x 1600 | 1600 x 1600 |
| 0.445 | 0.018 | 742 x 262 | 742 x 786 | 1600 x 1600 | 1600 x 1600 |
| 0.488 | 0.020 | 742 x 262 | 742 x 786 | 1600 x 1600 | 1600 x 1600 |
| 0.555 | 0.020 | 742 x 262 | 742 x 786 | 1600 x 1600 | 1600 x 1600 |
| 0.645 | 0.050 | 371 x 131 | 742 x 786 | 800 x 800 | 1600 x 1600 |
| 0.672 | 0.020 | 742 x 262 | 742 x 786 | 1600 x 1600 | 1600 x 1600 |
| 0.865 | 0.039 | 371 x 131 | 742 x 786 | 800 x 800 | 1600 x 1600 |
| 1.24 | 0.020 | 742 x 262 | 742 x 786 | 1600 x 1600 | 1600 x 1600 |
| 1.61 | 0.060 | 371 x 131 | 742 x 786 | 800 x 800 | 1600 x 1600 |
| 2.25 | 0.050 | 742 x 262 | 742 x 786 | 1600 x 1600 | 1600 x 1600 |

Each band has a calibration accuracy specification of 2%. The expected band noise performance provides signal-to-noise better than 100 for most cases, as illustrated in Figure 2.

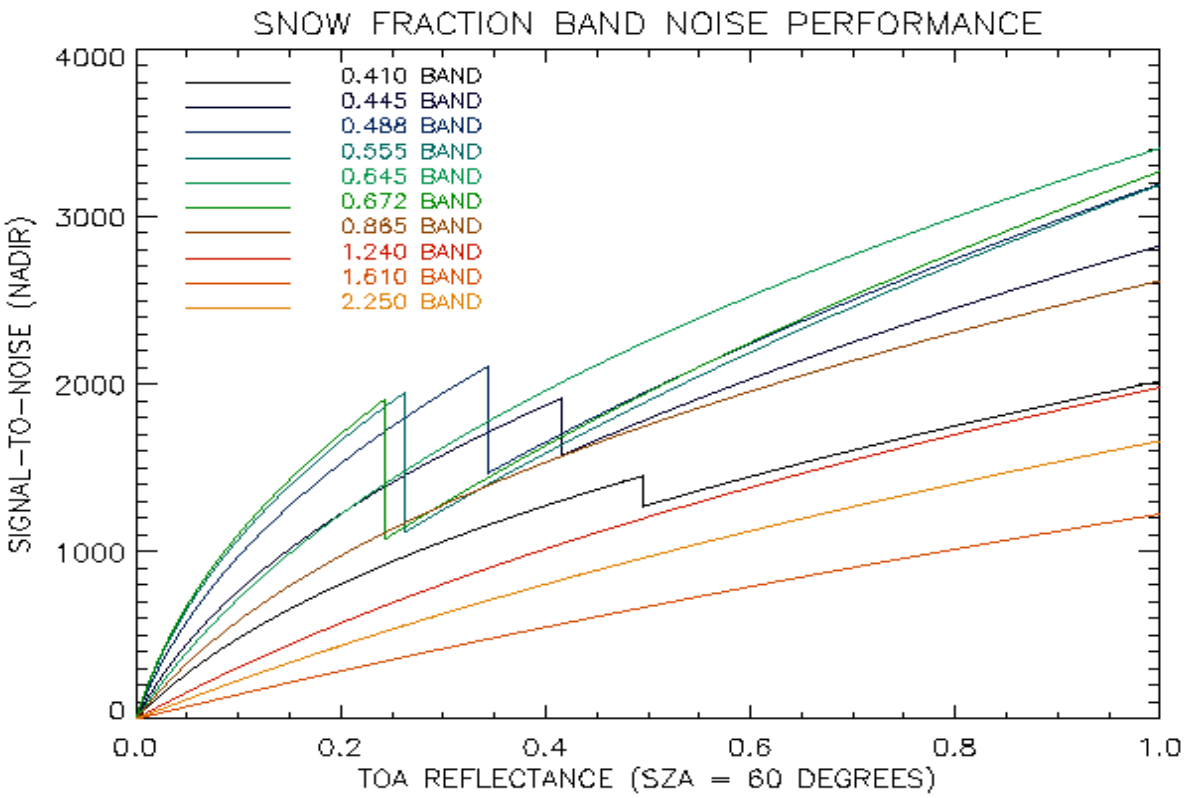


**Figure 2. Expected signal-to-noise performance for the three VIIRS fine resolution bands and 7 VIIRS moderate resolution bands used in the snow fraction algorithm.**

## 2.3 RETRIEVAL STRATEGY

### 2.3.1 Snow Binary Map

The input data will be an image cube, consisting of a two-dimensional grid of surface pixels for each of three VIIRS fine resolution bands in the form of geolocated surface reflectances. Surface reflectances will be supplied as a product of the Albedo EDR, as documented in the Atmospheric Correction Over Land algorithm *[Y2411]*.

The Cloud Mask algorithm *[Y2412]* will identify pixels that should be excluded from processing due to cloud or cloud shadow. The Cloud Mask will also supply a mask to identify boreal forest pixels requiring special consideration and a land/water mask.

Each pixel will be examined for its suitability. Pixels designated as land by the land/water mask and as clear or probably clear by the cloud mask will be passed for processing. Pixels designated as “probably clear” may have a quality flag attached to them. The solar/sensor angles for each pixel will be used to determine whether the pixel is rejected, passed for further processing with a quality flag attached, or passed for further processing without reservation.

Pixels which have been passed for processing will have their values of NDSI, NDVI, and NIR reflectance examined to determine a snow or no snow classification, following the prescription described in Section 3.3.2.

### 2.3.2 Snow Fraction

The input data will be an image cube, consisting of a two-dimensional grid of surface pixels for each VIIRS band in the form of geolocated surface reflectances. Surface reflectances will be supplied as a product of the Albedo EDR, as documented in the Atmospheric Correction Over Land algorithm *[Y2411]*. The ground imaged field of view (GIFOV) of each moderate resolution band is matched with all the other moderate resolution bands. The VIIRS fine resolution bands are nested with the VIIRS moderate resolution bands so that a 2 X 2 aggregate of fine resolution GIFOVs is matched with the GIFOV of the moderate resolution bands. The fine resolution reflectances will be averaged over the 2 X 2 aggregate corresponding to the GIFOV of the moderate resolution bands. The snow fraction algorithm uses all available reflectance band information, on the assumption that the relative weight of each band can be determined (c.f. Section 3.3.3). If each band contained completely independent information, the algorithm variance would scale as 1/N, where N is the number of bands. Because reflectance spectra contain band correlations, actual performance will not improve as much. Our performance analysis for snow fraction (c.f. Section 4.2.2) adopts the assumption that the bands are all completely correlated. To the extent that the suite of bands contain independent information, algorithm performance will improve.

The Cloud Mask algorithm *[Y2412]* will identify pixels that should be excluded from processing due to cloud or cloud shadow. The Build-SDR module *[Y3261]* will supply a mask to identify boreal forest pixels requiring special consideration and a land/water mask.

Each pixel will be examined for its suitability. Pixels designated as land by the land/water mask and as clear or probably clear by the cloud mask will be passed for processing. Pixels designated as “forest” by the forest mask will have a quality flag attached to them. Pixels designated as “probably clear” may have a quality flag attached to them. The solar/sensor angles for each pixel will be used to determine whether the pixel is rejected, passed for further processing with a quality flag attached, or passed for further processing without reservation.

The algorithm will acquire pixel-by-pixel information about non-snow spectral signatures from a reference database indicating the surface properties for the relevant month. Initially, we expect the database to be derived from MODIS and NPP. As the NPOESS mission progresses, we expect the database to be modified by the VIIRS observations, and provided as a Monthly Mean Non-snow Reflectance Intermediate Product (IP). The grid size of the monthly mean non-snow reflectance IP will be determined by the capabilities of MODIS and NPP, and by the capacity of the NPOESS system to store and access large databases. The smaller the grid size, the smaller will be the error in non-snow endmember reflectance.

For each pixel which has been passed for further processing, Multiple Endmember Spectral Mixture Analysis will be performed to derive snow fraction, following the prescription described in Section 3.3.3.

# 3.0 ALGORITHM DESCRIPTION

## 3.1 PROCESSING OUTLINE

The input surface reflectance data is tested for instrument quality, clear conditions, and solar zenith angle. All pixels which pass the tests are processed by the snow binary map algorithm (c.f. Section 3.3.2) and by the snow fraction algorithm (c.f. Section 3.3.3). The snow binary map algorithm produces a snow/no snow classification for each pixel, which is written to the EDR output. The snow fraction algorithm produces a snow fraction value for each pixel, which is also written to the EDR output. A description of the software process flow is in the VIIRS Snow/Ice Module Level Software Architecture document *[Y2477]*.

## 3.2 ALGORITHM INPUT

### 3.2.1 VIIRS Data

The snow binary map and snow fraction algorithms require the VIIRS data listed in Table 5.

**Table 5. VIIRS Data for the VIIRS Snow Cover Algorithms**

| Input Data | Source of Data | Reference |
|---|---|---|
| Instrument Quality | VIIRS RDR to SDR Processor* | *[Y3261]* |
| Geolocation | VIIRS Earth Location Algorithm | *[Y3258]* |
| Solar/Sensor Geometry | VIIRS RDR to SDR Processor* | *[Y3261]* |
| Surface Reflectance | VIIRS Atmospheric Correction Over Land Algorithm | *[Y2411]* |
| Cloud Mask | VIIRS Cloud Mask Algorithm | *[Y2412]* |
| Land/Water Mask | VIIRS Cloud Mask Algorithm | *[Y2412]* |
| Forest Mask | VIIRS Cloud Mask Algorithm | *[Y2412]* |
| Non-Snow Reflectance Spectra | VIIRS Monthly Mean Non-snow Reflectance IP* | *[Y2470]* |
| Snow Reflectance Spectra | Snow Reflectance LUT* | *[Y2470]* |

* RDR = Raw Data Record SDR = Sensor Data Record IP= Intermediate Product LUT= Look-up Table

#### 3.2.1.1 Instrument Quality

The Build-SDR module will attach instrument quality flags to the input data. Image pixels with one or more bad quality bands may have a snow fraction quality flag attached to them. Pre-launch or post-launch validation will determine which band losses require a snow fraction quality flag. A pixel with a bad SDR quality flag for any one of the three fine resolution bands will have a binary snow map quality flag attached to it.

#### 3.2.1.2 Geolocation

Geolocation of each imaged pixel will be used to report the latitude/longitude coordinate of each horizontal cell of the EDR product [*Y3258*].

#### 3.2.1.3 Solar / Sensor Geometry

Pixels with solar zenith angle greater than a threshold shall be excluded from further processing. Our current threshold is 80 degrees. Pixels with solar zenith angle between 70 degrees and 80 degrees will be processed, but with a quality flag attached. The final setting of these values will be made as part of the initialization plan (c.f. Section 3.6.1). Solar/sensor geometry may be used to apply a BRDF quality flag, if warranted by pre-launch or post-launch validation (c.f. Sections 3.6.2, 3.6.3).

#### 3.2.1.4 Surface Reflectance

The VIIRS Atmospheric Correction Over Land algorithm [*Y2411*] will produce surface reflectances for all bands used by the algorithms. Models of surface reflectance error are used in our error analysis (c.f. Section 3.4.2).

#### 3.2.1.5 Cloud Mask

The VIIRS cloud mask *[Y2412]* is expected to derive a status of clear/probably clear/probably cloudy/cloudy for each pixel, following the convention of the MODIS cloud mask (Ackerman *et al.*, 1997). Pixels flagged as "cloudy" will be excluded from further processing. We expect that pixels flagged as "probably cloudy" will also be excluded. This determination must depend on an assessment of the cloud mask performance, particularly over snow and ice surfaces. Pixels flagged as "probably clear" will be processed, although we wish to flag the output EDR as "possibly cloud contaminated." Pixels flagged as "definitely clear" will be processed. It is anticipated that the cloud mask will also flag pixels that are shadowed by clouds. In that case, a cloud shadow quality flag will be assigned to those pixels.

#### 3.2.1.6 Land/Water Mask

The EDR will be reported for land pixels. Coastline pixels must be identified and reported with a quality flag. The best quality land/water map available will be used. It is believed that a 1 km land/sea map will be developed by the EROS Data Center (EDC) from data products generated by the MODIS instrument. The land/water mask will be supplied as part of the Cloud Mask IP *[Y2412]*.

#### 3.2.1.7 Forest Mask

It is anticipated that a forest mask will be available. A forest canopy quality flag will be assigned to those pixels.

#### 3.2.1.8 Non-Snow Reflectance Spectra

Pixel-by-pixel information about non-snow spectral signatures will be acquired from a reference database indicating the surface properties for the relevant month. The database of non-snow reflectance will be available and corrected on the basis of the latest observations. Initially, we expect the database to be derived from MODIS heritage and improved by NPP. As the NPOESS mission progresses, it will be continually updated as a monthly mean non-snow reflectance IP.

#### 3.2.1.9 Snow Reflectance Spectra

Snow reflectance is variable, with a strong dependence on grain size and level of impurities. A reference library of model snow reflectances will be created as part of the initialization activity. The number and range of model spectra used will be determined by pre-launch validation activity (c.f. Section 5.1).

### 3.2.2 Non-VIIRS Data

The algorithms use no auxiliary and ancillary non-VIIRS data. Some non-VIIRS data is needed by the Cloud Mask algorithm *[Y2412]* and the Atmospheric Correction over Land algorithm *[Y2411]*. An account of these requirements is found in their ATBDs.

## 3.3 THEORETICAL DESCRIPTION OF THE RETRIEVAL

The processes outlined in Section 3.1 only apply to regions that have successfully passed the quality examinations. Descriptions of the mathematical backgrounds of these processes follow.

### 3.3.1 Physics of the Problem

Pure snow is a distinctive target across a part of the solar spectrum. It is among the brightest of natural substances in the visible and near-infrared part of the spectrum, but it is also often the darkest in the shortwave infrared (Dozier, 1989). The spectral albedo of snow depends on wavelength, and this dependency is controlled by the imaginary part *(k)* of the complex refractive index. This reaches a minimum at a wavelength of about 0.46 microns, and increases by a factor of $10^6$ - $10^7$ as wavelength increases out to 2.5 microns (Warren, 1982; Dozier, 1989). Light transmission decays exponentially in ice across a distance *d* as $\exp(-4\pi kd/\lambda)$. The *e*-folding distance for ice (the distance over which transmittance is reduced to 1/e) decreases from more than 20 m in the 0.4 – 0.5 micron range to less than 1 mm at 1.6 microns.

Light in snow is scattered primarily by refraction through, not reflection from, the ice grains. Photons are scattered at the grain surfaces, but absorbed while traversing the grain interiors. Only about 3 percent of the light scattered by an ice grain is reflected from the external surface. Nearly 89 percent is refracted through the grain, and 8 percent is scattered after internal reflections (Bohren and Barkstrom, 1974). Because ice is so transparent to visible radiation, snow reflectance is insensitive to grain size in bands below 0.7 microns, but sensitive to absorbing impurities in the snow and to SWE (Wiscombe and Warren, 1980; Grenfell, Perovich, and Ogren, 1981). Because absorption by ice is much stronger in bands above 1.4 microns, reflectance at these wavelengths is insensitive to absorbing impurities and SWE, but sensitive to

grain size. Absorbing particulates affect snow reflectance out to 0.9 microns (Warren and Wiscombe, 1980), so the 0.86 micron band is sensitive to both absorbing impurities and grain size. All aforementioned values in this paragraph are determined from geometric optics for a sphere.

The spectral signature of snow is unique among common substances. Clouds and snow are both bright across the visible and near-infrared region, but clouds are much brighter than snow in the shortwave infrared. This is because the smaller size of the scatterers in clouds decreases the probability of absorption in this spectral region where ice and water are moderately absorptive (Crane and Anderson, 1984; Dozier, 1984, 1989). Conversely, bodies of open water are dark at all wavelengths. Vegetation is dark in the visible bands because of absorption by photosynthetic pigments, but has a maximum reflectance between 0.7 and 1.3 microns. Because of leaf cell structure (Hoffer, 1978), shortwave infrared reflectance is inversely related to leaf water content for healthy vegetation. Nevertheless, the reflectance at wavelengthslonger than 1.5 microns is still high compared to that of snow. Most rock and soil spectra are the reverse of snow's. Absorption by iron oxides and organic matter strongly reduce visible reflectances, while those in the shortwave infrared remain high.

Typical reflectance properties of snow and other surfaces are illustrated in Figure 3. An illustration of snow/cloud reflectance differences is in Figure 4.

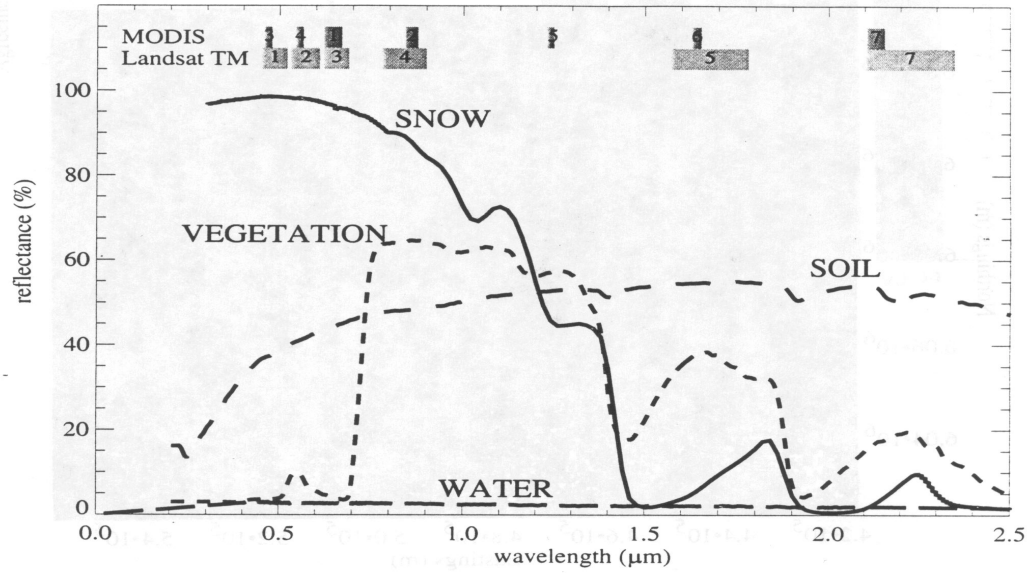


**Figure 3. Representative reflectance spectra for snow, vegetation, soil, and water (from Klein, Hall, and Riggs, 1998).**

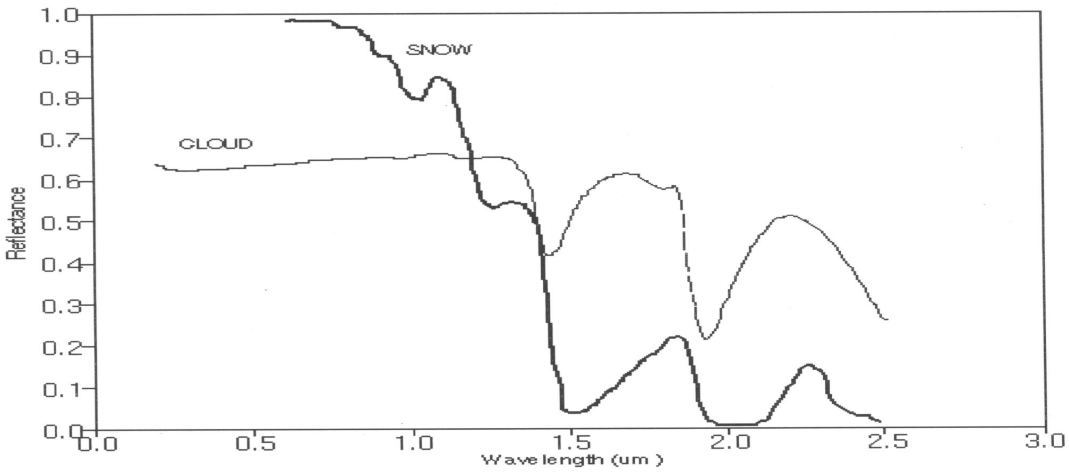


**Figure 4. Representative reflectance spectra for snow and clouds (from Hall *et al*., 1998).**

It is important to note that the reflectance spectra shown in the previous figures are representative of one typical case for each surface type and cloud type. Real surfaces will exhibit

spectral variability for any given surface type. In particular, snow reflectance depends on grain size and impurities. Cloud reflectance will vary with optical thickness, effective particle size, and phase.

The VIIRS Snow Cover EDR requirements apply to snow cover of any depth. Snow is such an efficient scatterer of visible and infrared radiation that the surface reflectance properties of snow are not very sensitive to snow depth or SWE. The physical basis for retrieval of snow depth or SWE is that the scattering efficiency of snow is measurably dependent on frequency in the passive microwave range of the spectrum. Microwave radiation upwelling from the underlying surface is scattered away from the sensor as it propagates through the snowpack. Thus, brightness temperatures at any given microwave frequency are lower for deeper snowpacks. In addition, the scattering efficiency increases with frequency over the microwave range. As a result, differences in brightness temperatures at different microwave frequencies are correlated with the SWE. This physical principle is the basis for SWE retrieval algorithms based on passive microwave observations (Grody and Basist, 1996; Foster, Chang, and Hall, 1997; Chang, 1998).

### 3.3.2 Mathematical Description of the Snow Binary Map Algorithm

The algorithm is an adaptation of the binary classification technique of the MODIS algorithm, SNOMAP (Hall *et al.*, 1998). SNOMAP classifies snow by a Normalized Difference Snow Index (NDSI) of 0.555 μm and 1.64 μm bands. Our algorithm is an adaptation of the MODIS algorithm. We use an NDSI from the 0.645 μm and 1.61 μm VIIRS fine resolution bands, combined with a reflectance threshold in the 0.865 μm VIIRS fine resolution band, to classify a VIIRS pixel as snow or non-snow at fine resolution.

$$NDSI = (R_1 - R_2) / (R_1 + R_2)$$

Where: $R_1, R_2$ = Reflectances in 0.645 μm, 1.61 μm MODIS bands

Pixels with an NDSI > 0.4 and a 0.865 μm reflectance > 0.11 are classified as snow. These thresholds have been developed from pre-launch MODIS characterization, as described in the MODIS ATBD (Hall *et al.,* 1998). An illustration of the application of these thresholds is shown as Figure 5.

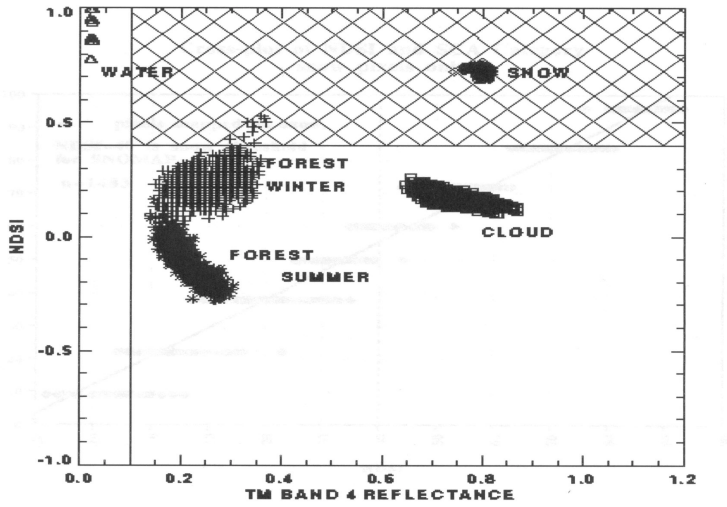


**Figure 5. Near-Infrared Reflectance versus NDSI plot for winter and summer Landsat TM scenes of Glacier National Park, Montana (from Hall et al., 1998). Pixels located in the cross-hatched region are classified as snow. Winter forest pixels, which are known to have snow cover under the forest canopy, are incorrectly classified as no snow.**

The MODIS algorithm also uses a Normalized Difference Vegetation Index (NDVI) to classify snow covered forest pixels by location in an NDSI/NDVI scatter plot.

$$NDVI = (R_1 - R_2) / (R_1 + R_2)$$

Where: $R_1, R_2$ = Reflectances in 0.858 μm, 0.645 μm MODIS bands

Pixels with 0.1 < NDSI < 0.4 are classified as snow cover under a forest canopy, if NDVI is greater than a threshold value. The threshold depends on the pixel NDSI. These thresholds have been developed from pre-launch MODIS characterization. A snow reflectance model was used in conjunction with a canopy reflectance model (GeoSAIL) to develop the thresholds, which were then tested on Landsat TM images of the southern BOREAS study area in Prince Albert National Park, Saskatchewan. Details can be found in Klein, Hall, and Riggs (1998). An illustration of the application of these thresholds is shown as Figure 6.

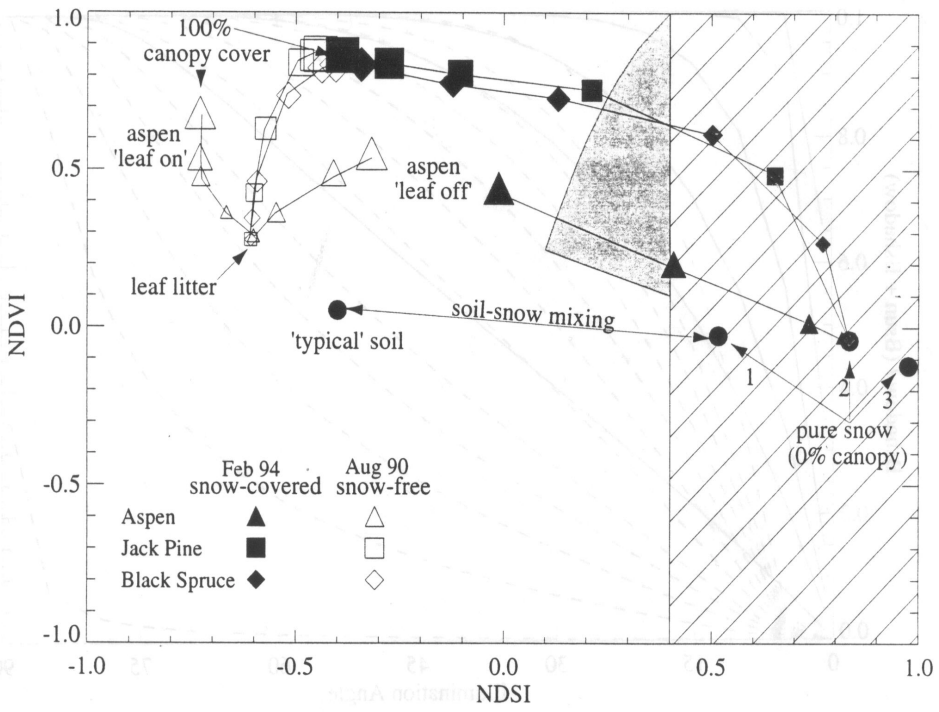


**Figure 6. NDSI versus NDVI plot for modeled aspen, jack pine, and spruce stands (from Klein, Hall, and Riggs, 1998). The hatched region is the snow classification region for the Version 4 MODIS algorithm. The gray shaded region represents a proposed additional region for capturing snow-covered forests.**

Our algorithm also adopts this approach.

### 3.3.3 Mathematical Description of the Snow Fraction Algorithm

The hypothesis that snow fraction can be determined by assuming that observed reflectance spectra are linear combinations of the spectra of a small set of scene components (spectral endmembers) has been supported by several studies (Nolin, Dozier, and Mertes, 1993; Rosenthal, 1993; Rosenthal and Dozier, 1996). These endmembers are the spectra of snow, rock, soil, or vegetation. They can be obtained from the image itself (image endmembers), or from calibrated field or laboratory spectra (reference endmembers). The algorithm to retrieve snow fraction includes an application of linear spectral unmixing. Spectral mixture analysis "unmixes" the mixed pixels determining the fraction of each spectral endmember that would combine to produce the mixed pixel's spectral signature.

Our approach is based on a mixture model which incorporates multiple snow endmembers to characterize subpixel snow cover. The technique is called Multiple Endmember Spectral Mixture Analysis (MESMA). Snow's spectral reflectance is sensitive to grain size, impurity, water content and other attributes. As a result, snow spectrally manifests itself as a range of endmembers. Thus, multiple snow endmembers are necessary to increase the accuracy of the snow cover retrieval. Use of multiple snow endmembers improves spectral mixture analysis. This approach is based on translation of varying snow parameters into different snow spectral reflectance. The variable spectral nature of snow is accounted for by use of multiple snow endmembers (Painter et al., 1998).

Significant sub-scene heterogeneity can contaminate SMA modeling with a fixed suite of endmembers. To increase the accuracy of the algorithm, we assume variation of the endmembers on a pixel-by-pixel basis. The algorithm takes into account the most prominent features of the endmember spectra varying from one location on the earth surface to another. We use MESMA allowing the endmembers to vary on a pixel-by-pixel basis, which accounts for variation in surface types both for snow and non-snow endmembers. Such an approach has been developed by Painter et al. (1998) and Roberts et al. (1998). It has been shown in these papers that reference endmember libraries can be used with great success to accurately map snow in alpine regions and in the Santa Monica Mountains.

Our approach is based on using a mixture model with known non-snow endmembers for each pixel. The snow cover (fraction) for the pixels is estimated by the mixture model with least mixing mean-square-root error. Our approach allows the types of snow endmembers to vary on a per pixel basis. It is assumed that the true reflectance is a linear combination of the non-snow reflectance and a single snow type reflectance:

$$M_{bt} = f\ S_{bt} + (1\text{-}f)\ X_b \qquad (3.3.3.1)$$

where: $f$ = True snow fraction.

$M_{bt}$ = Model reflectance in band (b) for snow type (t) and snow fraction (f).

$S_{bt}$ = Model reflectance in band (b) for snow type (t).

$X_b$ = Model non-snow reflectance in band (b).

The RMS variance of the observed reflectance from the model reflectance is:

$$e_t^2 = \Sigma \quad (R_b - f(S_{bt} - X_b) - X_b)^2 \; w_b \quad (t = 1,N) \qquad (3.3.3.2)$$

where: $R_b$ = Observed reflectance in band (b).

$w_b$ = Weight in band (b).

and the summation is over all bands.

Minimization of $e_t^2$ with respect to $f_t$ gives us the snow fraction for snow type (t):

$$f_t = \Sigma \quad (R_b - X_b)(S_{bt} - X_b) w_b \; / \quad \Sigma \quad (S_{bt} - X_b)^2 \; w_b \qquad (3.3.3.3)$$

where the summations are over all bands.

For each of the N snow types, the algorithm computes $f_t$ from equation (3.3.3.3). Fractions smaller than zero are set to zero. Fractions greater than one are set to one. The algorithm then computes $e_t^2$ by plugging $f_t$ back into equation (3.3.3.2). The type (t) with the smallest $e_t^2$ is selected, and its $f_t$ is reported as the snow fraction.

#### 3.3.3.1 Endmember Selection (Non-Snow Reflectance)

The construction of Equation 3.3.3.1 requires us to select the endmembers that constitute a given pixel in a scene. This is perhaps the largest constraint on the use of spectral unmixing as an operational approach to subpixel snow mapping.

Previous results of using MESMA (Roberts et al., 1998) show that a majority of the image could be modeled as two-endmember models. Three-endmember models provide poorer discrimination due to overlap of different models. Therefore, we limit our choice to two end-members. In general, the lower the number of endmembers, the higher the priority in choosing endmembers for SMA. But using MESMA along with the database of non-snow endmembers allows us to avoid constraints related to application of 2 endmembers.

The regional nature of endmembers presents the greatest hindrance for development of the algorithm. Our approach treats the non-snow endmember as an empirical quantity derived from observations, rather than a pure surface type.

Our proposed approach eliminates the search for endmembers on the fly, which significantly increases the speed of calculations, making possible operational usage. Optimal speed and efficiency are achieved when the information on non-snow endmember reflectance is available and accurate. Features of non-snow endmembers change from pixel to pixel. The reflectance spectral signatures of non-snow endmembers are a source of error, since the conditions of the underlying surface at a particular location will vary seasonally.

MESMA has been successful in regional mapping of snow fraction. Given this success, there is good reason to expect the technique can be developed so that it is operational on a global basis.

There is some risk associated with applying the algorithm globally, since the required global database of non-snow reflectance does not currently exist.

We plan to grow a global library of monthly mean non-snow reflectance in the VIIRS bands to account for seasonal variations. The library will be built from satellite observations rectified to a fixed latitude/longitude grid. MODIS will produce a surface reflectance product (Vermote, 1999), which will be used to build an initial database. The MODIS bands are similar to the VIIRS bands. Rectification of the MODIS data to the VIIRS bands should therefore introduce minimal error. Observations during the NPP will build on the MODIS database and customize it to the VIIRS bands.

#### 3.3.3.2 Snow Reflectance

The reflectance spectral signatures of snow endmembers will be obtained from a reference database, which we will build. There are different ways to collect information on snow spectral signatures. These include analytic derivations from scattering theory, observations under laboratory conditions, *in situ* observations, and remote observations from orbiting satellites.

We plan to rely primarily on *in situ* observations, which are available from numerous field observations of snow reflectance.

Remote observations have the advantage that they are obtained in a similar way to the VIIRS data, but they are subject to errors in atmospheric correction. We will rely on a VIIRS atmospheric correction to surface reflectance, and will not use previous satellite observations to build our database.

Observations under laboratory conditions do not reproduce the wide variety of possible snow conditions found in nature.

Analytic derivations use simplifying assumptions to make them tractable. We will use these as a quality check on the *in situ* observations.

### 3.3.4 Archived Algorithm Output

The binary snow map will be archived as a yes/no bit for each pixel. The retrieved fraction of snow for each VIIRS pixel will be archived as a floating point number.

Data quality flags will be attached to any reported product derived from input data with a data quality flag attached. These include, but are not necessarily limited to, data flagged as “probably clear”, “cloud shadow”, and “forest canopy”.

# 4.0 EDR PERFORMANCE

The performance of the algorithms with respect to the VIIRS requirements and the System Specification (c.f. Tables 1 and 2) is reviewed in this section.

EDR performance shall be verified by analysis, modeling, and/or simulation based on the instrument design and performance characteristics and the algorithms. The analysis, modeling, and/or simulation shall be sufficiently extensive in scope to verify that EDR requirements are met under a broad range of conditions that are representative of those occurring in nature, include typical and extreme conditions.

## 4.1 STRATIFICATION

### 4.1.1. Snow Binary Map

We identify the following stratifications for the snow binary map:

- Snow fraction “truth”
- Sensor view angle
- Solar zenith angle
- Fraction of mixed pixels

Performance of the snow binary map algorithm will depend on snow fraction. The probability of correct typing for any binary classifier must approach 50% as the threshold for defining yes/no “truth” is approached. Our algorithm thresholds have been tuned to a threshold of 0.5 in snow fraction. That is, the probability of correct typing will increase as true fraction differs from 0.5. A sensible stratification must then include snow fraction “truth” as a parameter. We have selected 5 ranges of snow fraction, 0.0-0.2, 0.2-0.4, 0.4-0.6, 0.6-0.8, and 0.8-1.0. We have deliberately selected these ranges so that they are symmetric with respect to 0.5, where we expect minimum EDR performance.

The requirements are specified at nadir. Our stratification of sensor view angle is restricted to nadir view.

We have used a solar zenith angle of 60 degrees in our simulations to date. Our stratification of solar zenith angle is restricted to this value. A wider range of solar zenith angles shall be simulated in the future, following the development of surface reflectance error simulations over a wider range.

It is informative to report EDR performance for a representative range of structured scenes. We parameterize this range as a stratification by fraction of mixed pixels in a scene. Scenes with a greater fraction of mixed pixels are expected to have a reduced EDR performance because spatial errors (MTF, band misregistration) are greater and because the binary classifier must degrade as snow fraction approaches 0.5. We have selected three stratifications by fraction of mixed pixels, 10% (easy), 30% (typical), and 50% (hard).

### 4.1.2 Snow Fraction

We identify the following stratifications for the snow fraction:

- Snow fraction "truth"
- Sensor view angle
- Solar zenith angle
- Fraction of mixed pixels

Performance of the snow fraction algorithm is expected to depend on snow fraction ("truth"). We have selected 4 ranges of snow fraction, 0.0-0.25, 0.25-0.5, 0.5-0.75, and 0.75-1.0.

Unlike the binary snow map, the snow fraction requirements are specified at worst case as well as nadir. Our stratification of sensor view angle includes nadir and edge-of-scan views.

We have used a solar zenith angle of 60 degrees in our simulations to date. Our stratification of solar zenith angle is restricted to this value. A wider range of solar zenith angles shall be simulated in the future, following the development of surface reflectance error simulations over a wider range.

It is informative to report EDR performance for a representative range of structured scenes. We parameterize this range as a stratification by fraction of mixed pixels in a scene. Scenes with a greater fraction of mixed pixels are expected to have a reduced EDR performance because spatial errors (MTF, band misregistration) are greater. We have selected three stratifications by fraction of mixed pixels, 10% (easy), 30% (typical), and 50% (hard).

## 4.2 STRATIFIED PERFORMANCE ANALYSIS

### 4.2.1. Snow Binary Map

Performance verification is by demonstration.

We classified MODIS Airborne Simulator (MAS) scenes as snow or no snow at a 50 meter pixel resolution, with the aid of an unsupervised 6 band classification in ENVI. Manual review of the ENVI classifications was performed to assign each ENVI-derived class as snow or no snow.

We aggregated each scene to pixel sizes of 0.4 km and 0.8 km to simulate VIIRS pixels at nadir and edge of scan respectively. We classified each VIIRS pixel as snow or no snow, depending upon the number of snow/no snow MAS pixels in the aggregate. At nadir, a VIIRS pixel is an aggregate of 64 MAS pixels. For a VIIRS nadir pixel to be classified as snow, it required 33 or more MAS pixels classified as snow. For a VIIRS nadir pixel to be classified as no snow, it required 33 or more MAS pixels classified as no snow. These classifications are used as "VIIRS truth".

A number of perturbations were applied to the scenes to simulate sensor/algorithm performance.

Reflectance errors were applied to the scenes. We perturbed the aggregated reflectances in MAS bands 3 (648 nm), 7 (866 nm), and 10 (1.63 μm), using model errors for the Surface Reflectance IP in VIIRS bands 5i (645 nm), 6i (865 nm), and 8i (1.61 μm). We have obtained these from the performance analysis of the Atmospheric Correction Over Land algorithm *[Y2411]*. Reflectance accuracy errors were modeled by assuming an aerosol optical thickness (AOT) of 0.1 and a 0.05 offset between true AOT and the AOT acquired from a climatological database. Details on the creation and use of the aerosol climatology are found in the Atmospheric Correction over Land ATBD *[Y2411]*.Our selection of AOT mean and offset is based on studies of typical aerosol conditions in the sub-arctic (Blanchet and List, 1983). Reflectance precision errors were modeled from the sensor noise performance specification. The reflectance errors depend on surface reflectance truth, which is correlated with snow fraction. Reflectance errors were calculated for a solar zenith angle of 60 degrees.

Spatial errors were also applied to the scene. The scenes were perturbed by MTF smearing, following the sensor MTF performance specification. Band misregistration was simulated by offsetting the NIR and SWIR bands by 0.2 pixels with respect to the visible band, consistent with the VIIRS sytem specification for band registration *[PS154640-101]*.

We applied the algorithm to the perturbed VIIRS scenes to retrieve snow/no snow, and computed probability of correct typing by comparing the retrieved classifications to the “VIIRS truth”. We did this for four scenes:

1) A Death Valley scene containing no snow cover (SUCCESS_115_16)

2) A Brazil scene containing no snow cover (SCAR-B_163_1)

3) A Northern Minnesota scene containing 100% snow cover under a varying canopy (WINCE_49_06)

4) A mixed snow/no snow scene in Colorado in February (WINCE_50_14)

The first two scenes test the algorithm performance over desert and vegetated non-snow surfaces. The third scene tests the performance in winter forest regions. The fourth scene tests the performance for a typical case of mixed snow/no snow pixels.

**Death Valley Scene**: Visible (.645 μm) and SWIR (1.6 μm) images of the scene are shown in Figure 7. There is of course no snow in the scene. The bright feature is a salt pan. It can not be distinguished from snow by the visible data alone (Figure 7a), but its brightness in the SWIR (Figure 7b) does distinguish it from snow.

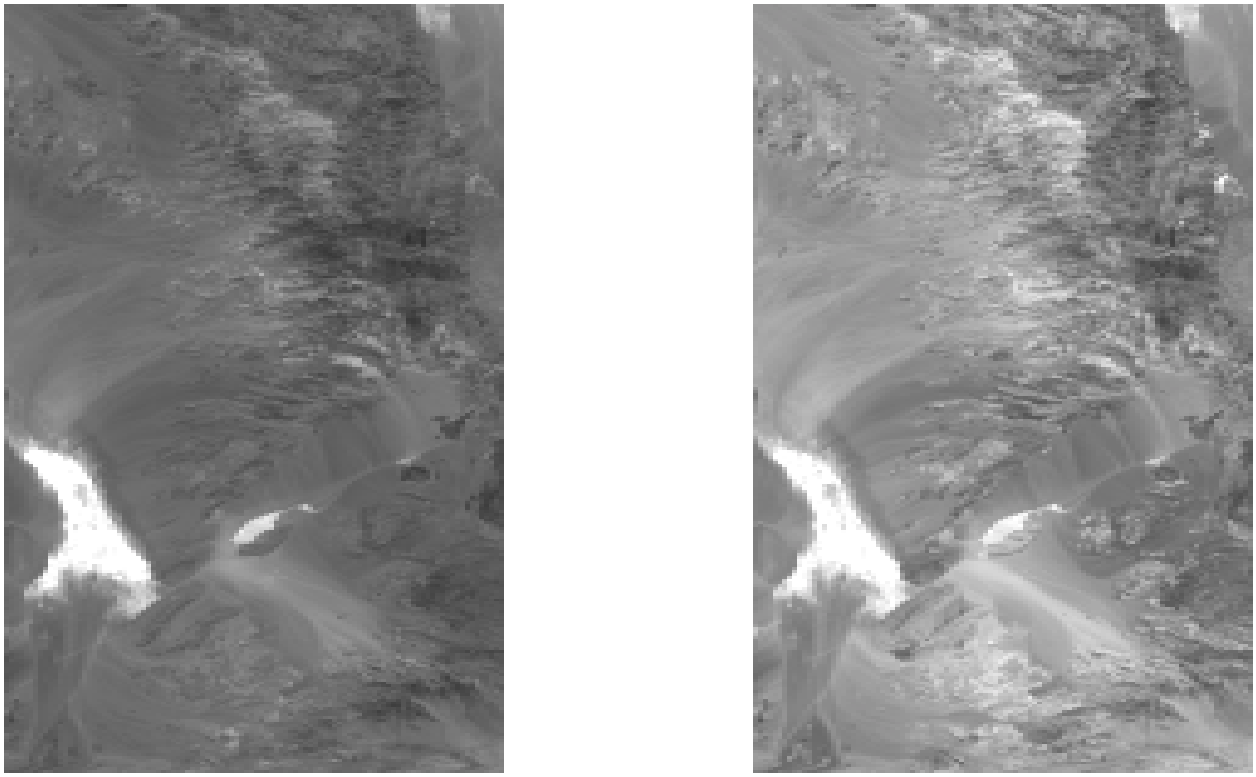

**(a)** **(b)**

**Figure 7. (a) Visible reflectance image of Death Valley scene from MAS/SUCCESS campaign. The grey-scale is from 0.0 to 0.5 in reflectance. (b) Short Wave IR reflectance image of the scene. The grey-scale is from 0.0 to 0.5 in reflectance.**

The NDSI/NDVI scatter plot for the Death Valley scene is shown in Figure 8. Expected system performance errors were added to the scenes.

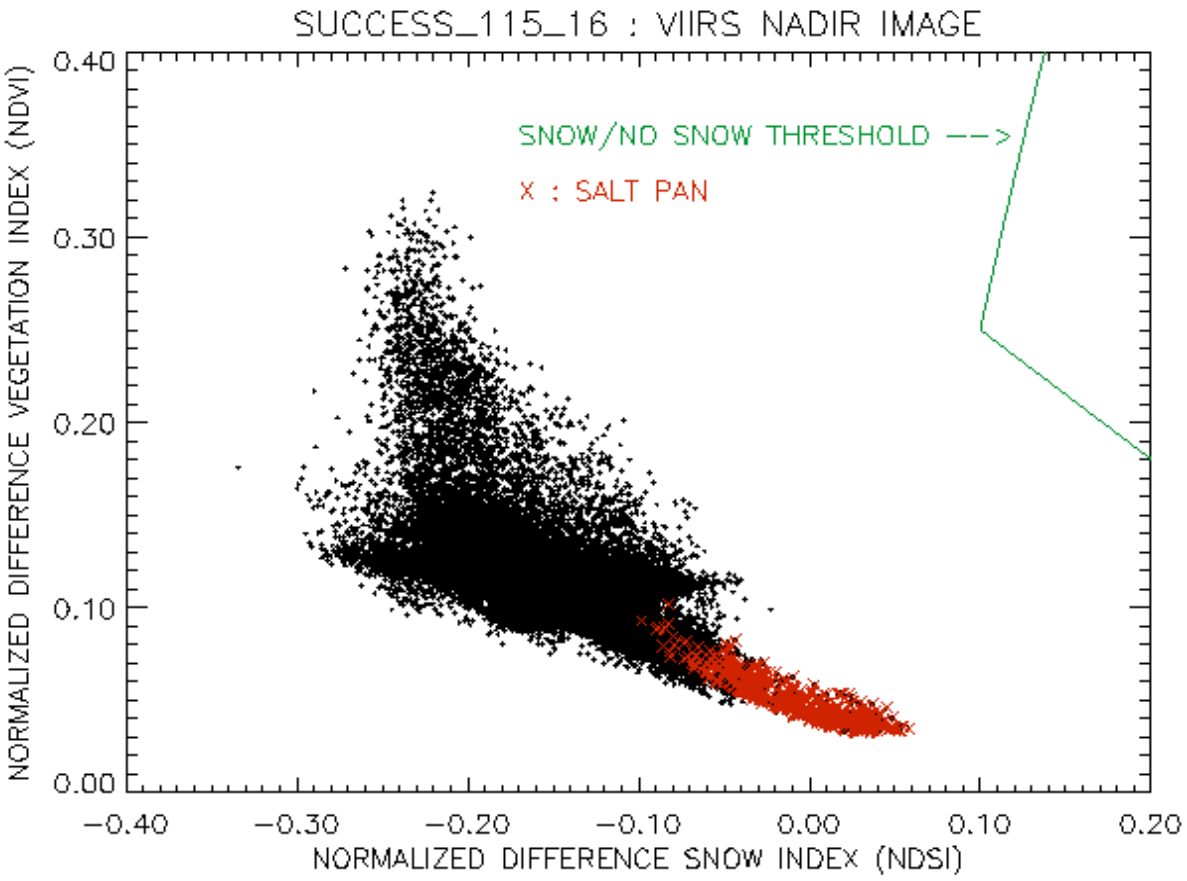


**Figure 8. NDSI versus NDVI scatter plot of the MAS Death Valley scene (SUCCESS_115_16). The image has been aggregated to a VIIRS pixel size at nadir.**

Correct classification occurs when pixels classified as snow fall to the right of the green threshold boundary and when pixels classified as no snow fall to the left of the boundary. All pixels in this scene were correctly classified as no snow, including the salt pan.

**Brazil Scene**: Visible (.645 μm) reflectance, NDVI, and NDSI images of the scene are shown in Figure 9. There is of course no snow in the scene.

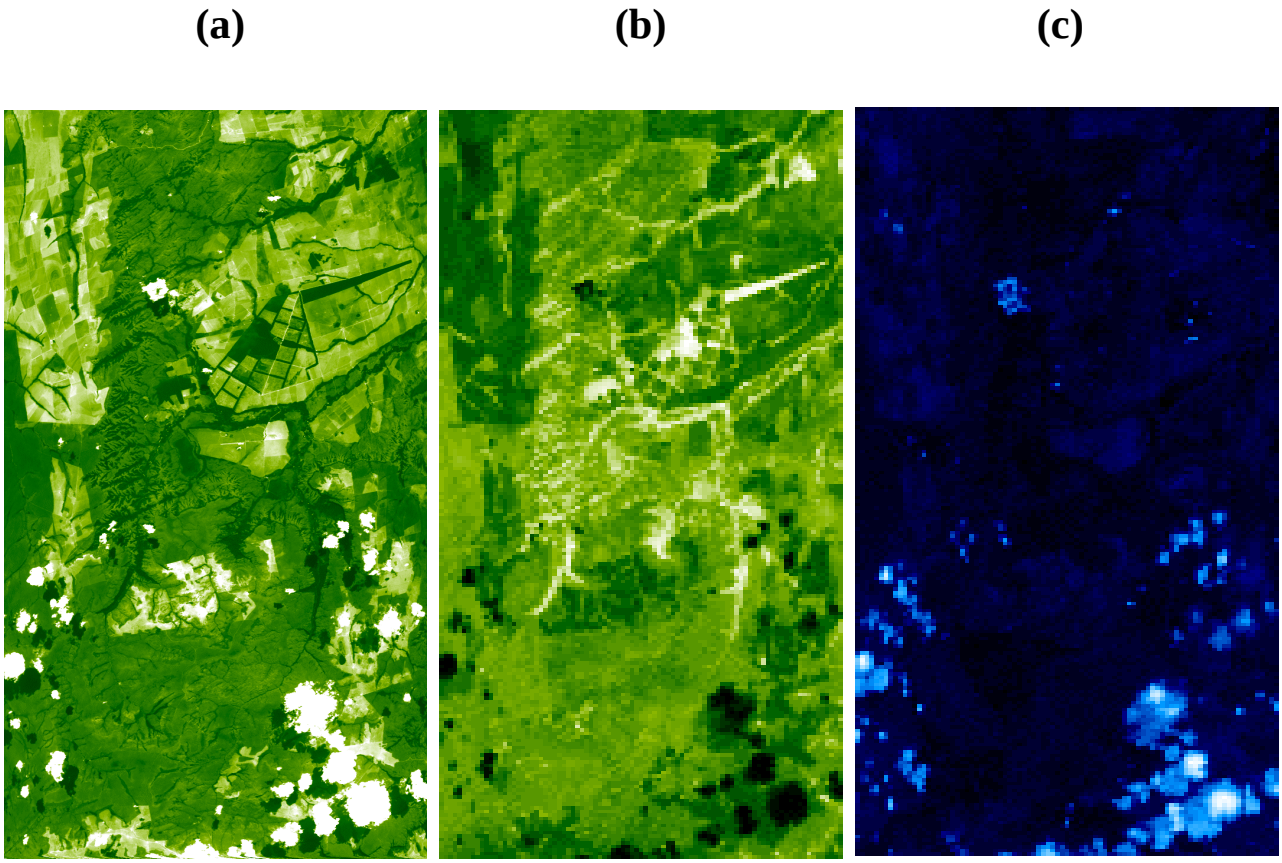


**Figure 9: (a) Visible reflectance image of Brazil scene from MAS/SCAR-B campaign. The color scale is from 0.0 to 0.2 in reflectance. (b) NDVI image of the scene. The color scale is from 0.05 to 0.7 in NDVI units. (c) NDSI image of the scene. The color scale is from –0.5 to 0.07 in NDSI units.**

The NDSI/NDVI scatter plot for the Brazil scene is shown in Figure 10. Expected system performance errors were added to the scenes.

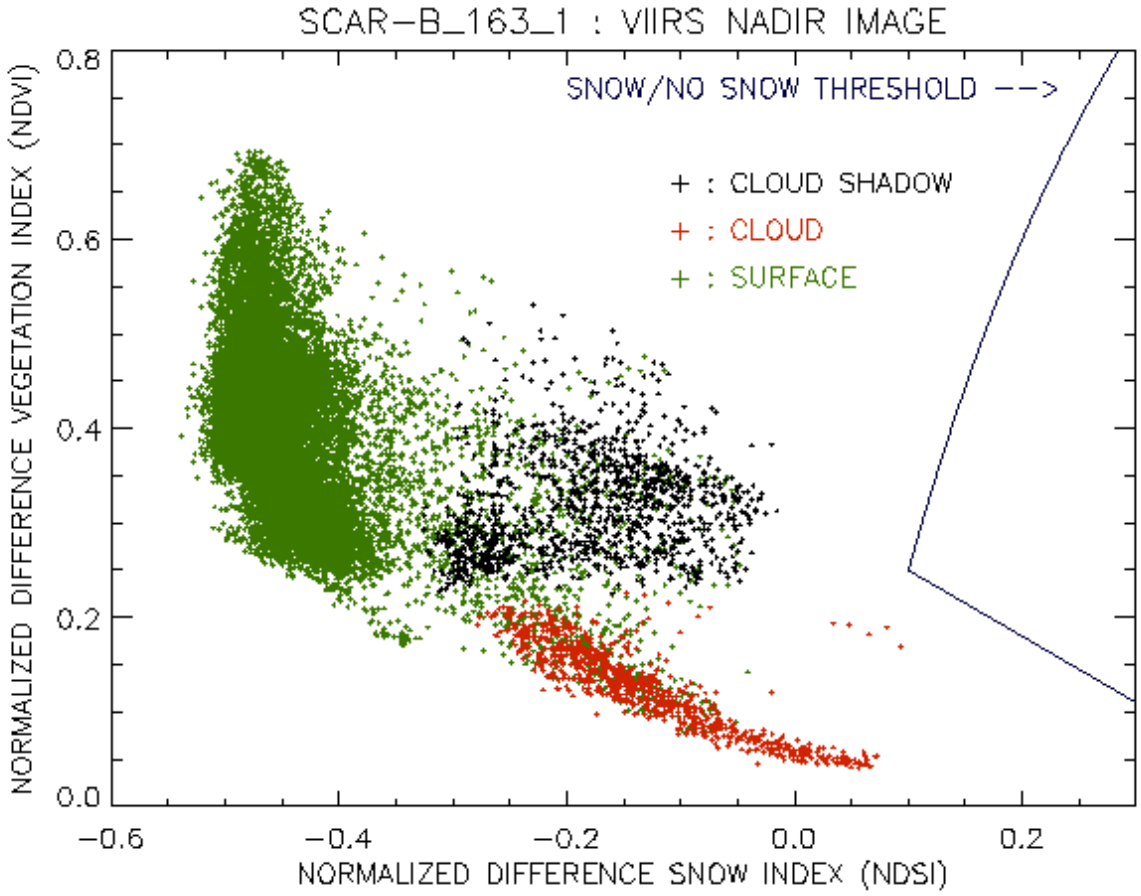


**Figure 10. NDSI versus NDVI scatter plot of the MAS Brazil scene (SCAR-B_163_1). The image has been aggregated to a VIIRS pixel size at nadir.**

Correct classification occurs when pixels classified as snow fall to the right of the blue threshold boundary and when pixels classified as no snow fall to the left of the boundary. All pixels in this scene were correctly classified as no snow, including the cloud and cloud shadow pixels.

**Minnesota Winter Scene:** Visible (.645 μm) reflectance is shown in Figure 11a. Manual review of the ENVI-classified scene has established that the scene is 100% snow covered. The large variation in reflectance is caused by a variation in the forest canopy over the snow covered surface. The NDSI image is shown in Figure 11b. Brighter areas have larger NDSI. These areas have a lighter forest canopy. The NDVI image is shown in Figure 11c. Darker areas have larger NDVI. These areas have a denser forest canopy.

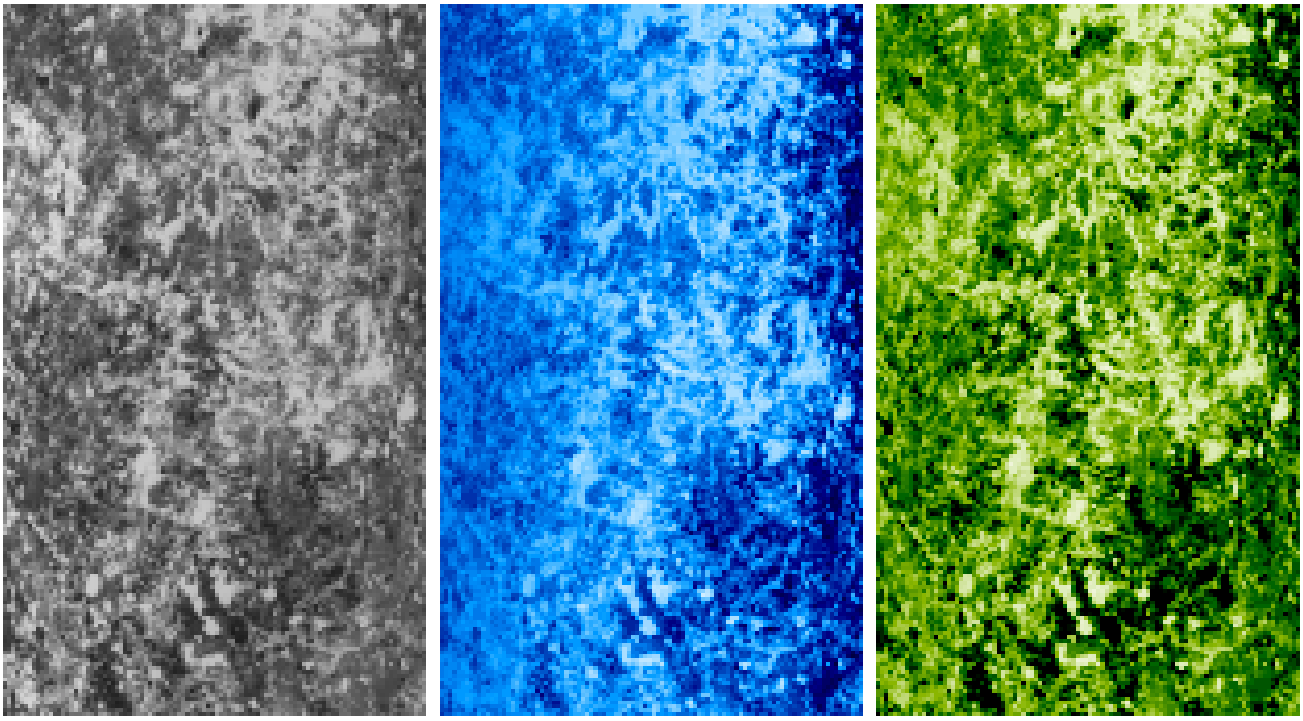

**Figure 11. (a)Visible reflectance image of Minnesota winter scene from MAS/WINCE campaign. The grey-scale is from 0.0 to 1.0 in reflectance. (b) Normalized Difference Snow Index (NDSI) image of the scene. The color scale is from NDSI = 0.0 (darkest) to NDSI = 0.8. (c) Normalized Difference Vegetation Index (NDVI) image of the scene. The color scale is reversed, from NDVI = 0.25 (darkest) to NDVI = 0.05.**

The NDSI/NDVI scatter plot for the MAS Minnesota winter scene is shown in Figure 12. Expected system performance errors were added to the scene. All of the VIIRS pixels were correctly classified as snow.

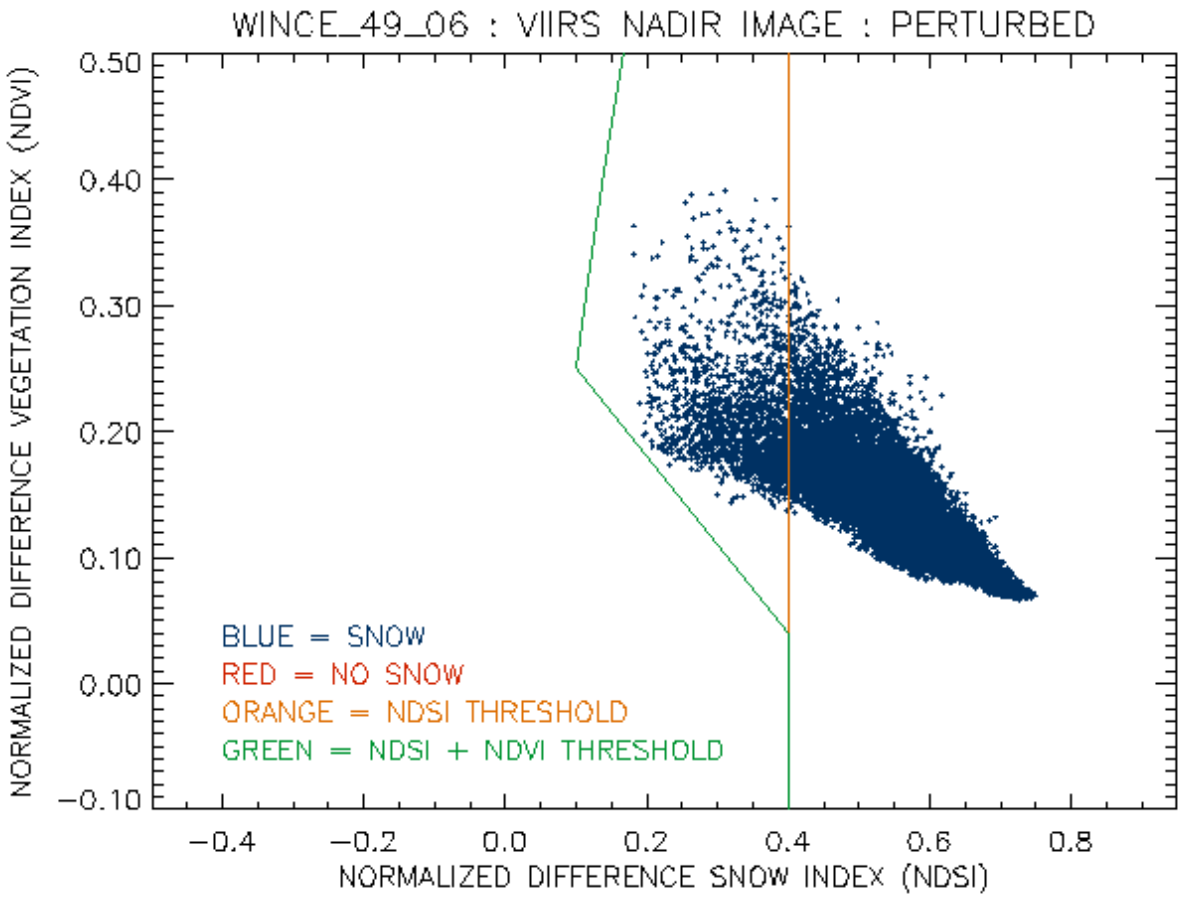


**Figure 12. NDSI versus NDVI scatter plot of the MAS Minnesota winter scene (WINCE_49_06). The image has been aggregated to a VIIRS pixel size at nadir.**

Comparison of this figure to Figure 11 indicates that the scene can be characterized as a uniform snow-covered surface under a variable forest canopy. As the density of the canopy increases, the location in the scatter plot moves up and to the left, resulting in a canopy-density track. Correct classification occurs when pixels classified as snow (blue) fall to the right of the green threshold boundary and when pixels classified as no snow (red) fall to the left of the boundary. All pixels in this scene are correctly classified as snow. Without the NDVI correction, misclassification would occur where blue pixels fall to the left of the orange boundary, resulting in a correct classification of 91.6 %.

**Colorado Winter Scene:** Visible (.645 μm) reflectance is shown in Figure 13a. Manual review of the ENVI-classified scene has established that the scene has a mixture of snow cover. Aggregation of the classified pixels to a VIIRS nadir resolution produces a snow fraction "truth" image, shown in Figure 13b. The scene was perturbed by our model for system error, and our binary map algorithm applied to the perturbed data. The result is shown in Figure 13c.

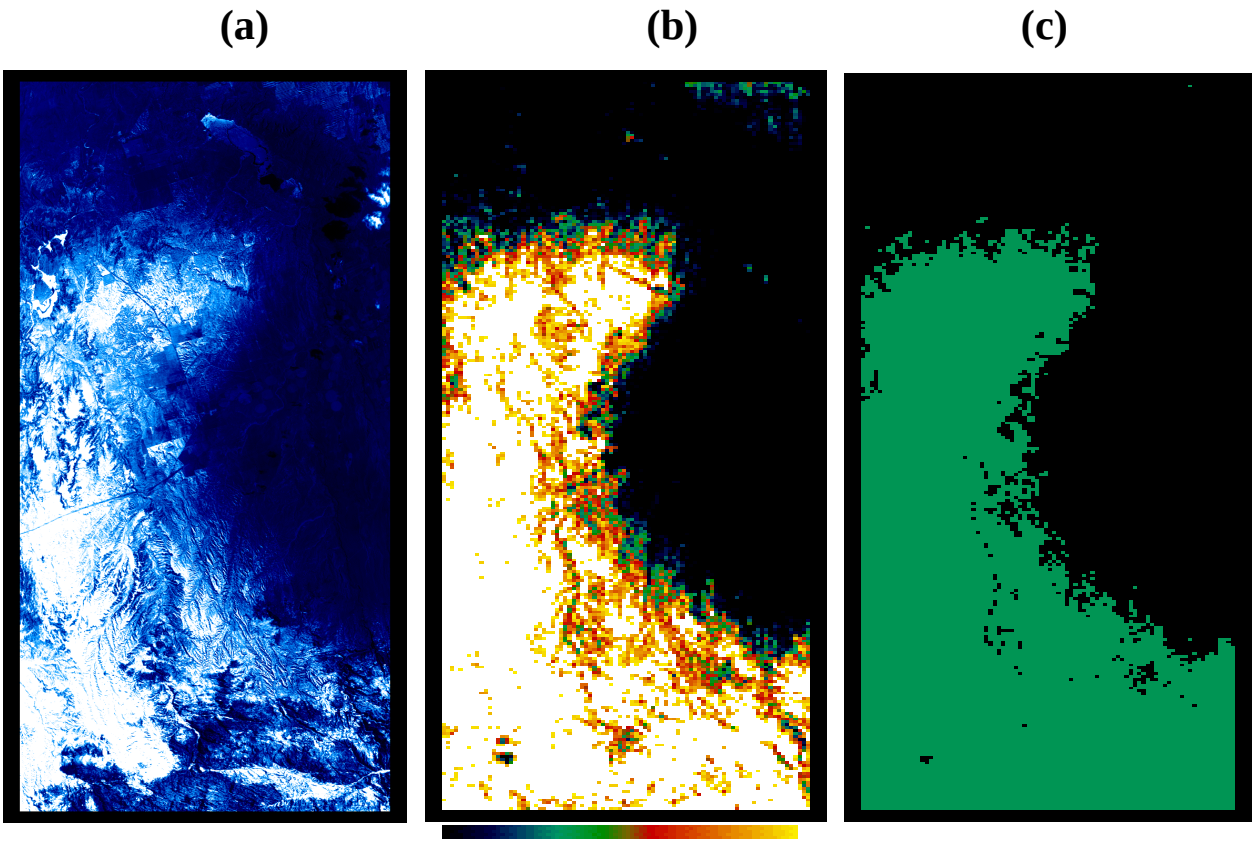


**Figure 13. (a) Visible Reflectance at 50 meter resolution, taken from a 0.648 micron image of Eastern Colorado obtained by the MODIS Airborne Simulator (MAS) on February 13, 1997. The extent of the scene is 35 km x 100 km. (b) Snow fraction at 0.4 km resolution, obtained by classification and aggregation to a VIIRS pixel size at nadir. (c) Retrieved Binary Snow Cover map. System performance errors were used to simulate a VIIRS retrieval. Green cells are mapped as snow. 97.8 % of the pixels were correctly typed.**

Figure 14 shows an NDSI versus NDVI scatter plot for the Colorado winter scene, aggregated to a VIIRS pixel size at nadir, with no error perturbations.

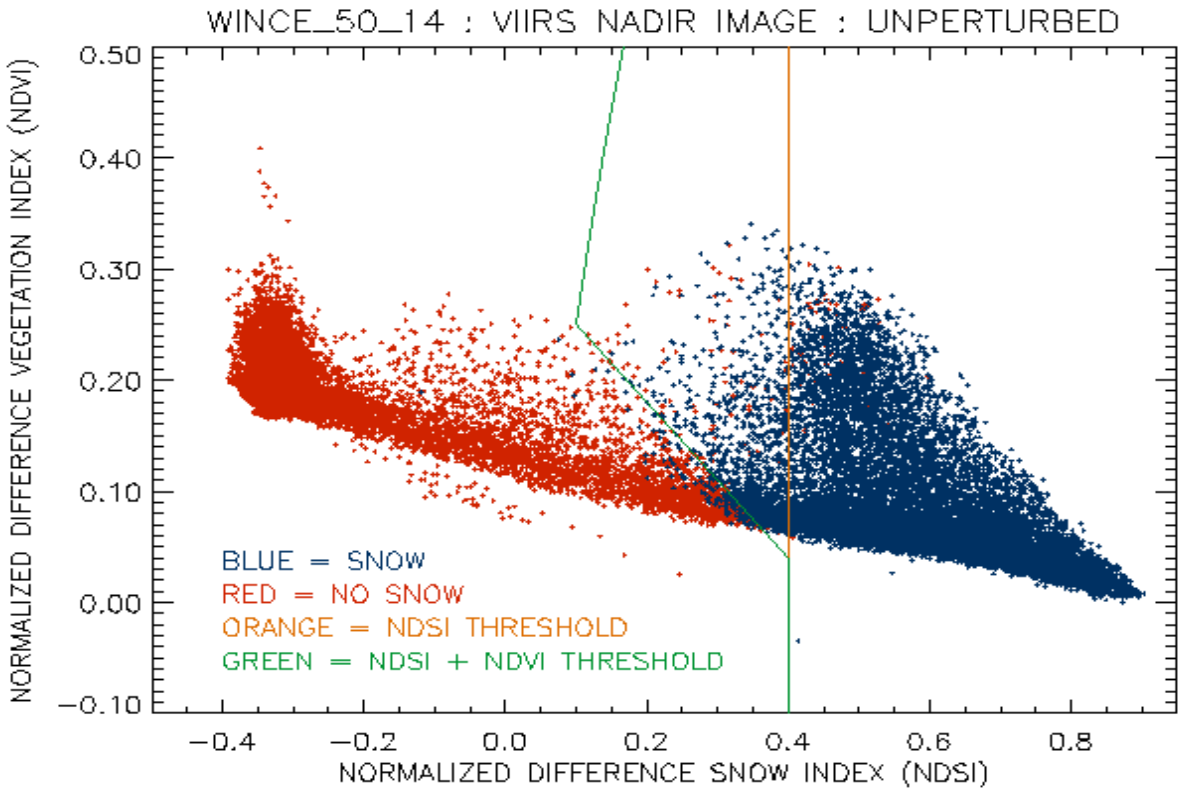


**Figure 14. NDSI versus NDVI scatter plot of the MAS Colorado winter scene (WINCE_50_14). The image has been aggregated to a VIIRS pixel size at nadir.**

Correct classification occurs when pixels classified as snow (blue) fall to the right of the green threshold boundary and when pixels classified as no snow (red) fall to the left of the boundary. Correct classification occurs for 98.52 % of the pixels. Without the NDVI correction, additional misclassification would occur where blue pixels fall to the left of the orange boundary.

Figure 15 shows an NDSI versus NDVI scatter plot for scene 1, aggregated to a VIIRS pixel size at nadir, with error perturbations (atmospheric correction, sensor noise, sensor MTF, band misregistration) added.

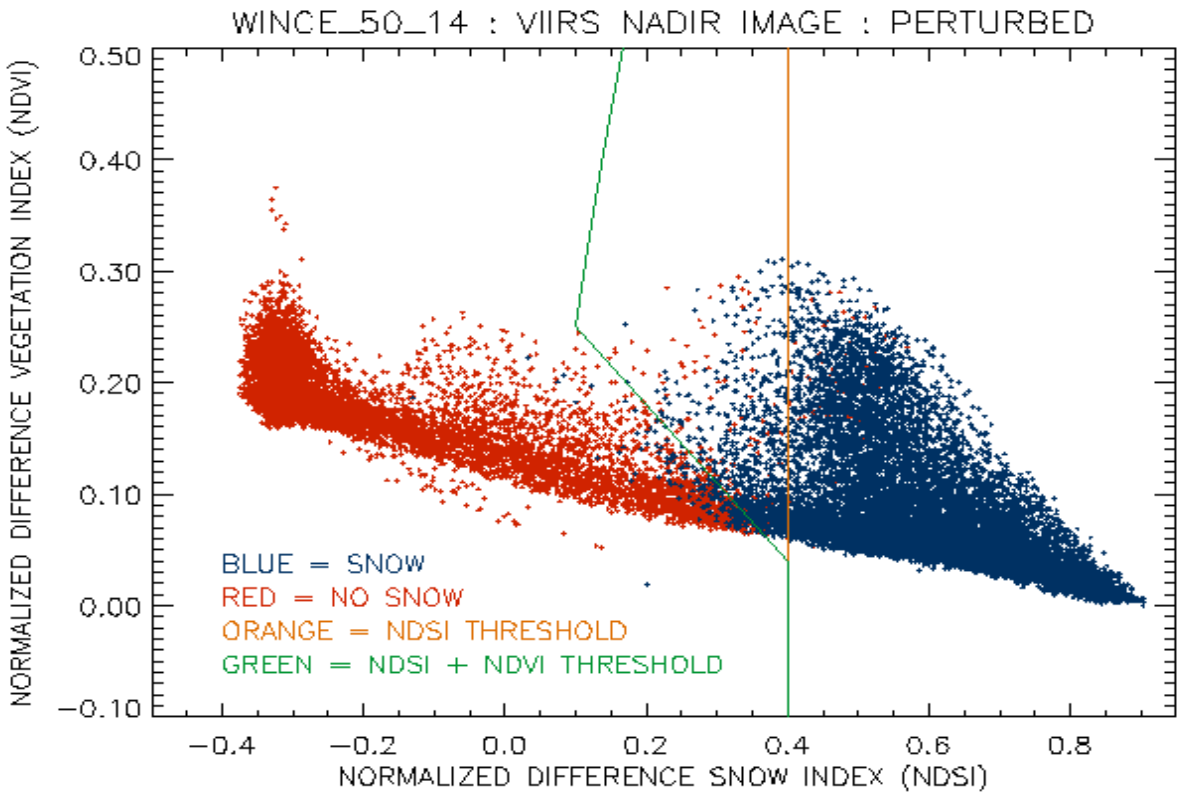


**Figure 15. NDSI versus NDVI scatter plot the MAS Colorado winter scene (WINCE_50_14). The image has been aggregated to a VIIRS pixel size at nadir. Error perturbations have been added to the scene.**

Correct classification occurs when pixels classified as snow (blue) fall to the right of the green threshold boundary and when pixels classified as no snow (red) fall to the left of the boundary. Correct classification occurs for 97.79 % of the pixels. Without the NDVI correction, additional misclassification would occur where blue pixels fall to the left of the orange boundary.

The probability of correct typing for scene 4 is illustrated as a function of snow fraction truth in Figure 16.

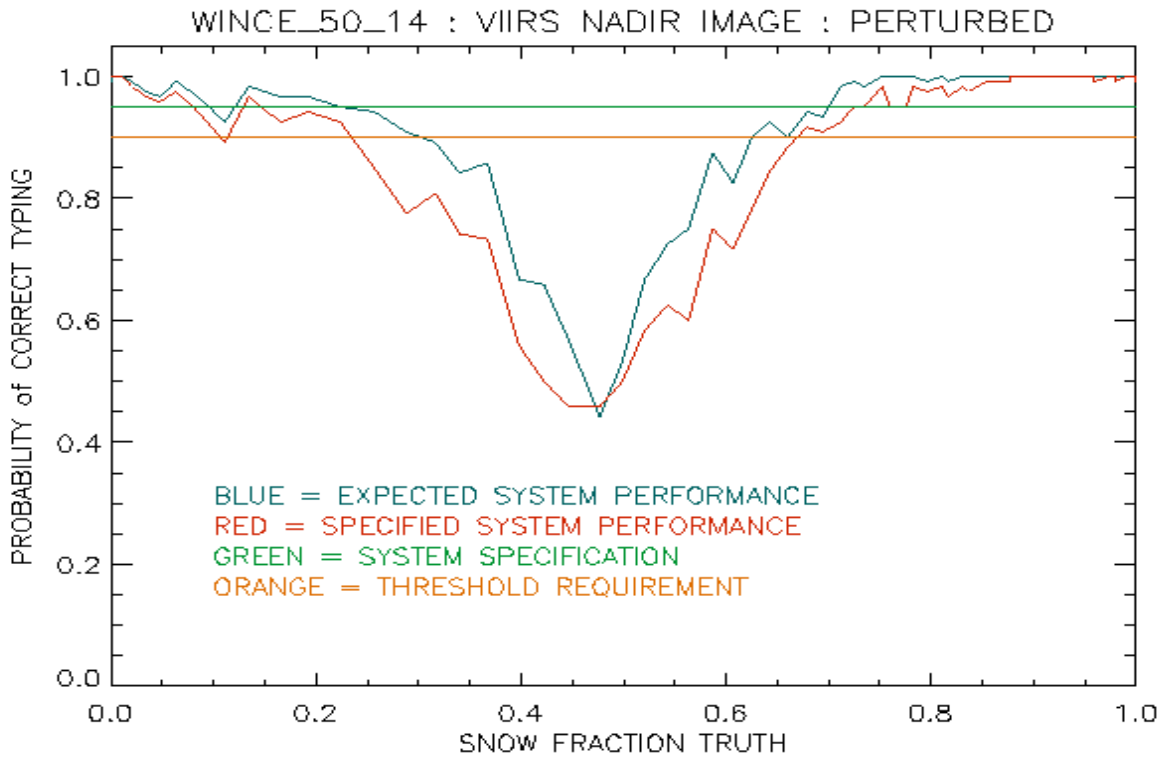


**Figure 16. Probability of Correct Typing vs. Snow Fraction for the MAS Colorado winter scene (WINCE_50_14). The scene was aggregated to a pixel size of 0.4 km to simulate a VIIRS nadir view.**

Results from the analysis of the Colorado mixed snow cover scene have been incorporated into a stratified performance summary, shown in Table 6

**Table 6. Snow Binary Map : Probability of Correct Typing (%) Clear, Nadir, SZA = 60 degrees, Some Canopy, Mixed Snow/No Snow**

| | Snow Fraction (Truth) | | | | | Fraction of Mixed Pixels | | |
|---|---|---|---|---|---|---|---|---|
| | 0.0 – 0.2 | 0.2 – 0.4 | 0.4 – 0.6 | 0.6 – 0.8 | 0.8 – 1.0 | 10% | 30% | 50% |
| Specification | 99.36 | 80.56 | 56.74 | 92.07 | 99.88 | 99.04 | 97.12 | 95.20 |
| Performance | 99.60 | 89.95 | 66.51 | 96.35 | 99.99 | 99.37 | 98.13 | 96.89 |

An explanation of the stratification bins is in Section 4.1.1. Probability of correct typing for each of the "truth" bins was derived by examining the classification error for the subset of pixels falling into the "truth" range of the given bin. Probability of correct typing for each of the "fraction of mixed pixels" bins was derived in the following manner. The probability of correct typing for pure pixels was calculated by examining the classification error for the subset of pure pixels. The probability of correct typing for mixed pixels was calculated by examining the classification error for the subset of mixed pixels. The probability of correct typing for a given fraction of mixed pixels is calculated as the weighted mean of the pure pixel and mixed pixel probabilities, with the mixed pixel weight equal to the fraction of mixed pixels.

It is important to note that the probability of correct typing for any binary classifier must approach 50% when the "truth" approaches 0.5. The performance results shown in Figure 16 and Table 6 reflect this characteristic. The practical measure of performance is for a realistic distribution of true fraction for various scenes, as is shown in the last three columns of Table 6.

### Snow Binary Map Error Budgets

The various error sources have been incorporated into error budgets for easy, typical, and difficult cases. These are shown in Tables 7, 8 and 9.

**Table 7. Error Budget for Retrieval of the Snow Binary Map EDR**

| SNOW COVER (Snow Binary Map)<br>Case: Clear, Nadir, SZA = 60 degrees, 10% Mixed Pixels (Easy case) | | |
|---|---|---|
| **Specification v3 (PDR)** | **Probability of Correct Typing (%)** | **Reference** |
| Threshold | 90.00 | VIIRS SRD |
| Objective | N/A | |
| A-Specification | 95.00 | Raytheon VIIRS Specification v3 |
| Predicted Performance | 99.37 | Raytheon VIIRS Specification v3 |
| Margin | 95.60 | Raytheon VIIRS Specification v3 |
| Algorithm B-Specification | 99.55 | Raytheon VIIRS Specification v3 |
| Thresholds | 99.58 | Raytheon VIIRS Specification v3 |
| Atmospheric Correction | 99.98 | Raytheon VIIRS Specification v3 |
| Sensor B-Specification | 99.81 | Raytheon VIIRS Specification v3 |
| Sensor Noise | 99.96 | Raytheon VIIRS Specification v3 |
| MTF | 99.84 | Raytheon VIIRS Specification v3 |
| Band Misregistration | 99.85 | Raytheon VIIRS Specification v3 |

**Table 8. Error Budget for Retrieval of the Snow Binary Map EDR**

| SNOW COVER (Snow Binary Map)<br>Case: Clear, Nadir, SZA = 60 degrees, 30% Mixed Pixels (Typical case) | | |
|---|---|---|
| **Specification v3 (PDR)** | **Probability of Correct Typing (%)** | **Reference** |
| Threshold | 90.00 | VIIRS SRD |
| Objective | N/A | |
| A-Specification | 95.00 | Raytheon VIIRS Specification v3 |
| Predicted Performance | 98.13 | Raytheon VIIRS Specification v3 |
| Margin | 96.81 | Raytheon VIIRS Specification v3 |
| Algorithm B-Specification | 98.67 | Raytheon VIIRS Specification v3 |
| Thresholds | 98.74 | Raytheon VIIRS Specification v3 |
| Atmospheric Correction | 99.93 | Raytheon VIIRS Specification v3 |
| Sensor B-Specification | 99.43 | Raytheon VIIRS Specification v3 |
| Sensor Noise | 99.89 | Raytheon VIIRS Specification v3 |
| MTF | 99.52 | Raytheon VIIRS Specification v3 |
| Band Misregistration | 99.55 | Raytheon VIIRS Specification v3 |

**Table 9. Error Budget for Retrieval of the Snow Binary Map EDR**

| SNOW COVER (Snow Binary Map)<br>Case: Clear, Nadir, SZA = 60 degrees, 50% Mixed Pixels (Hard case) | | |
|---|---|---|
| **Specification v3 (PDR)** | **Probability of Correct Typing (%)** | **Reference** |
| Threshold | 90.00 | VIIRS SRD |
| Objective | N/A | |
| A-Specification | 95.00 | Raytheon VIIRS Specification v3 |
| Predicted Performance | 96.89 | Raytheon VIIRS Specification v3 |
| Margin | 98.05 | Raytheon VIIRS Specification v3 |
| Algorithm B-Specification | 97.80 | Raytheon VIIRS Specification v3 |
| Thresholds | 97.91 | Raytheon VIIRS Specification v3 |
| Atmospheric Correction | 99.89 | Raytheon VIIRS Specification v3 |
| Sensor B-Specification | 99.04 | Raytheon VIIRS Specification v3 |
| Sensor Noise | 99.82 | Raytheon VIIRS Specification v3 |
| MTF | 99.20 | Raytheon VIIRS Specification v3 |
| Band Misregistration | 99.25 | Raytheon VIIRS Specification v3 |

If the various error sources listed in tables 7, 8, and 9 were completely uncorrelated, the combination of probabilities would follow the formula:

$$P = P_1 \times P_2 \times \ldots \times P_N$$

Because the various error sources contain some correlation, the probabilities do not combine in this way. To derive the error budgets, we used multiple simulated images. Each simulated image contained one and only one of the perturbations. Comparison of retrieval with truth for each of the simulations gave us the error contribution of the associated perturbation. To simulate the easy, typical, and difficult cases, we computed separate errors for pure pixels and mixed pixels, and weighted accordingly.

The largest error is the "thresholds" error. This error is caused by the limitations of our limited threshold tests in accounting for the real variety of surface and canopy reflectance. In principle, the error could be reduced by improvements in canopy modeling and by the use of different thresholds for different surface types. Because our performance is significantly better than the SRD requirement, we do not at present see the necessity to deviate from the MODIS approach.

Finally, we note that the sensor signal-to-noise performance is better than the specification. For the 1.6 micron band, the improvement is substantial. Because sensor noise is such a small component of the error budget, EDR performance would still meet specification if the sensor signal-to-noise were degraded to its specification values. For example, if we replace sensor noise performance with sensor noise specification, our probability of correct typing for our hard case degrades from to 96.88 % to 95.20 % (c.f. Table 9).

### 4.2.2 Snow Fraction

Verification of the performance of the snow fraction algorithm is by analysis and simulation.

Errors in snow fraction are produced by errors in surface reflectance, model snow reflectance, and model non-snow reflectance, as can be seen from equation (3.3.3.3). Our flowdown studies suggest that spatial errors (MTF and band misregistration) are important for scenes where mixed snow cover is variable on spatial scales comparable to the horizontal cell size. To simulate these errors, we have analyzed MAS scenes of mixed snow cover.

For our error analysis, we have assumed equally weighted bands. Optimal band weighting can in principle reduce our errors.

**Errors in Model Snow Reflectance:** The algorithm selects the snow reflectance model which minimizes the RMS error. Deviation of the model spectrum from the "true" snow reflectance introduces error. We have performed simulations to quantify this error. We adopted 10 models of snow reflectance, ranging from grain sizes of 50 microns to 1000 microns. We selected a MAS scene of mixed snow cover and retrieved a snow/no snow classification for each MAS pixel, using the snow binary map algorithm. We aggregated the classified MAS pixels to VIIRS pixel sizes to obtain "true" snow fraction. For each MAS pixel classified as snow, we simulated 1000 "real" reflectance spectra by random interpolation between the models. That is, we assumed that the combination of a random fraction of each of the 10 types is an adequate model for "true"

reflectance from the snow cover in a pixel. For each pixel classified as no snow, we used the observed reflectance. We aggregated the reflectances to VIIRS pixel size and performed the snow fraction retrieval, using the 10 model snow spectra and the observed non-snow spectra. The RMS snow fraction measurement uncertainty was 0.02, computed by comparison of the retrieved snow fractions to the "true" snow fraction.

**Errors in Model Non-Snow Reflectance:** The non-snow reflectance will be obtained from an external database of monthly mean non-snow reflectance. This database does not exist at present. The plan is to establish the database from MODIS data, and to continually update it during the NPP and NPOESS missions. We have simulated the performance of the database by using the average observed non-snow spectrum in a 6 km cell surrounding a given pixel as a proxy. This produces an error of 0.04 in snow fraction. We adopt this error in our budget, but note that the quantification of this error source will require verification. Verification will require the MODIS data.

**Errors in Surface Reflectance:** We have obtained these from the performance analysis of the Atmospheric Correction Over Land algorithm *[Y2411]*. The errors depend on surface reflectance truth, which is correlated with snow fraction. Reflectance errors were calculated for a solar zenith angle of 60 degrees, an aerosol optical thickness of 0.1, an error in aerosol optical thickness of 0.05, and a calibration bias of 2%, to simulate expected system performance for a typical solar zenith angle and atmosphere.

**MTF Errors:** Errors due to MTF smearing of the radiances have been analyzed. Our test scenes were MODIS Airborne Simulator scenes of mixed snow cover. Ground truth was determined at 50 meter spatial resolution. We adopted a sensor GIFOV of 1.3 km at 3000 km swath, subjected the scenes to an MTF smearing derived from the current VIIRS baseline sensor performance model, retrieved snow cover with our algorithm, and computed Measurement Uncertainty. For a scene with 50% mixed pixels, the error in snow fraction due to MTF was 0.064. We adopt a linear scaling of MTF error with fraction of mixed pixels, so that the estimated MTF error for scenes with 30% mixed pixels is 0.039.

**Band Misregistration Errors:** We applied a band misregistration of 0.2 pixels, following the VIIRS system specification for band-band registration *[SS154640-001]*. For a scene with 50% mixed pixels, the error in snow fraction was 0.037. As with MTF, we adopt a linear scaling of error with fraction of mixed pixels, so that the estimated band misregistration error for scenes with 30% mixed pixels is 0.022.

Tables 10, 11, and 12 show the errors stratified by scan angle, and snow fraction truth for easy, typical, and hard cases.

**Table 10. Snow Fraction Measurement Uncertainty : Clear, 10% Mixed Pixels (Easy case)**

| Scan Angle | Snow Fraction (Truth) | | | |
|---|---|---|---|---|
| | 0.0 – 0.25 | 0.25 – 0.5 | 0.5 – 0.75 | 0.75 – 1.0 |
| Nadir | .053 | .056 | .061 | .067 |
| Edge-of-Scan | .061 | .065 | .077 | .091 |

**Table 11. Snow Fraction Measurement Uncertainty : Clear, 30% Mixed Pixels (Typical case)**

| Scan Angle | Snow Fraction (Truth) | | | |
|---|---|---|---|---|
| | 0.0 – 0.25 | 0.25 – 0.5 | 0.5 – 0.75 | 0.75 – 1.0 |
| Nadir | .070 | .072 | .076 | .081 |
| Edge-of-Scan | .077 | .079 | .089 | .102 |

**Table 12. Snow Fraction Measurement Uncertainty : Clear, 50% Mixed Pixels (Hard Case)**

| Scan Angle | Snow Fraction (Truth) | | | |
|---|---|---|---|---|
| | 0.0 – 0.25 | 0.25 – 0.5 | 0.5 – 0.75 | 0.75 – 1.0 |
| Nadir | .096 | .097 | .100 | .104 |
| Edge-of-Scan | .100 | .102 | .110 | .121 |

An explanation of the stratification bins is in Section 4.1.2.

#### 4.2.2.1 Snow Fraction Error Budget

The various error sources for a typical case have been incorporated into an error budget, shown in Table 13.

**Table 13. Error Budget for Retrieval of the Snow Fraction EDR**

| SNOW COVER (Snow Fraction)<br>Case: Clear, Nadir, SZA = 60 degrees, 30% Mixed Pixels, Truth = 0.5 | | |
|---|---|---|
| **Specification v3 (PDR)** | **Measurement Uncertainty** | **Reference** |
| Threshold | N/A | |
| Objective | 0.1000 | VIIRS SRD |
| A-Specification | 0.1000 | Raytheon VIIRS Specification v3 |
| Predicted Performance | 0.0738 | Raytheon VIIRS Specification v3 |
| Margin | 0.0675 | Raytheon VIIRS Specification v3 |
| Algorithm B-Specification | 0.0587 | Raytheon VIIRS Specification v3 |
| Surface Reflectance | 0.0380 | VIIRS Snow Cover/Depth ATBD v3 |
| Snow Reflectance | 0.0200 | VIIRS Snow Cover/Depth ATBD v3 |
| Non-Snow Reflectance | 0.0400 | VIIRS Snow Cover/Depth ATBD v3 |
| Sensor B-Specification | 0.0450 | Raytheon VIIRS Specification v3 |
| MTF | 0.0390 | VIIRS Snow Cover/Depth ATBD v3 |
| Band Misregistration | 0.0220 | VIIRS Snow Cover/Depth ATBD v3 |

## 4.3 LIMITS OF APPLICABILITY

In this section, we discuss the conditions under which our EDR specified performance can not be attained.

### 4.3.1 Cloudy

The VIIRS Snow Cover EDR is required under clear conditions only, with clear defined as a cloud optical thickness less than 0.03. Our specification is for clear scenes only. Clouds are not amenable to spectral mixture analysis, because their reflectance properties are highly variable. The standard approach to minimize errors caused by clouds is to mask pixels where clouds are likely to be present in the radiance path. The VIIRS Cloud Mask *[Y2412]* will perform this function. Because no cloud mask is perfect, there will be some source of error caused by the effects of unmasked clouds. Thin clouds will perturb the upwelling surface reflected radiance by absorption, and scattering, and will also be a source of reflected and radiance unrelated to the surface. There will also be error due to incorrect classification of cloud contaminated pixels as clear as well as due to cloud shadows.

It is desirable to perform tests to determine the expected size of the retrieval errors under various conditions of cloud optical thickness and phase. Thin cirrus clouds are a particularly important case of cloud error, because they are particularly difficult for the cloud mask to detect over snow.

These tests require the simulation of TOA radiances from snow surfaces with a variety of overlying cloud layers. It has not been feasible to perform these tests to date because the VIIRS Cloud IPT requires a stable sensor design to make the simulations. In the absence of these tests, we cannot quantify the effect of clouds. The conditions under which the specification can not be attained may include a range of cloud optical thickness. The range will be determined by a balance between the increasing effect of clouds on the signal and the increasing probability of correct masking. The specification of this range has been deferred to future validation activity.

### 4.3.2 Low Light or Nighttime

The algorithm requires solar reflectance. Thermal contrast between snow and non-snow land surfaces is not a characteristic property. A solar zenith angle threshold of 80 degrees is adopted. For larger angles, surface reflectance errors become too large. Improved atmospheric correction would allow us to increase this threshold. The extension and refinement of the threshold is a goal of pre-launch initialization. MODIS experience will be of great value.

### 4.3.3 Forest canopy (snow fraction)

A large part of snow cover occurs in the boreal forests. These forests obscure most of the underlying surface. Observations of forest canopy under conditions where 100 percent snow cover is expected show albedo variations as large as 70%. Snow cover measurement uncertainties of 10% are not possible under these conditions. We have to be able to identify and flag pixels of forest canopy. The binary snow map algorithm will perform in boreal forests. We have verified its performance for the winter forest canopy of Northern Minnesota. Its performance in the deeper boreal forests is TBD. MODIS validation is expected to thoroughly characterize the performance in boreal forests.

## 4.4 PRACTICAL CONSIDERATIONS

### 4.4.1 Numerical Computation Considerations

The requirement to retrieve EDRs on a global, operational basis in a 20-minute time frame places constraints on the SMA technique. The algorithms have been run on a UNIX server under controlled conditions to verify compatibility with the operational requirements.

### 4.4.2 Programming and Procedural Considerations

All procedures must be automatic, in order to perform in the operational environment. It is expected that the algorithms will be directed by decision nodes, based on the availability and quality of data, as well as on regional and seasonal considerations. Therefore, all LUTs and decision trees that may be required must be available at all times.

### 4.4.3 Configuration of Retrievals

The Snow Cover EDR expects the output from the VIIRS Cloud Mask IP and the VIIRS Albedo EDR. The NPOESS processing configuration should be designed to satisfy these expectations.

### 4.4.4 Quality Assessment and Diagnostics

Quality flags will be attached to each archived pixel result. The snow fraction algorithm will produce an error estimate for each pixel. The algorithm should be expected to archive the final pixel errors for quality assessment. Ideally, a pixel error greater than an accepted threshold will be flagged.

In principle, quality assessment can be incorporated into the algorithm as a factor affecting decision nodes. For example, the persistence of large pixel errors could trigger an alternative technique for non-snow endmember selection.

### 4.4.5 Exception Handling

Pixels identified by the cloud mask will be flagged. Pixels with bad quality flags will be skipped and flagged. Bands with bad quality flags will be removed.

# 5.0 INITIALIZATION AND VALIDATION

## 5.1 INITIALIZATION

Our plan is to establish and maintain close contact with the MODIS teams, following the selection phase of the NPOESS program, to coordinate our initialization activity with their post-launch validation.

Plans include the development of a reliable global reference database of non-snow endmembers. The development the database will be an ongoing project. We expect the MODIS and NPP missions to accumulate information on surface constituents and their reflectance spectra for various global locations and times of year. A MODIS Surface Reflectance product (Vermote, 1999) is expected to be stored at the MODIS DAAC. The product will contain the surface reflectances, corrected for atmosphere and BRDF, for MODIS bands 1 and 2 at 250 meter resolution, and bands 3-7 at 500 meter resolution. This database should be more than sufficient to establish a monthly mean non-snow reflectance database for VIIRS at a fixed latitude/longitude grid of 1 km.

We will create a global database of monthly mean non-snow reflectance in the MODIS reflectance bands from MODIS data. The reflectances will be corrected to VIIRS bands by spectral interpolation. The corrected database will be used at the start of the NPP mission. As the NPP mission proceeds, the database will be continually updated from NPP observations. We expect a smooth transition from MODIS to NPP to NPOESS.

We will also extend our library of snow reflectance spectra. Our current library spans a reasonable range of snow grain sizes, but does not account for the effects of impurities. It is expected that the capabilities of the planned GLI mission will provide useful data for this activity.

Radiative transfer models will be applied to large solar zenith angle data to optimize the models for polar conditions, and to develop decision rules for solar zenith angle thresholds. MODIS data taken at solar zenith angles greater than 70 degrees will be studied to fine tune our solar zenith angle threshold for daytime conditions. The limiting factor is believed to be the reliability of atmospheric correction at larger solar zenith angles. Plane parallel radiative transfer algorithms are inaccurate for angles greater than 70-75 degrees. Development of improved radiative transfer models at larger angles will allow us to relax this constraint. To solve the Radiative Transfer Equation appropriately one would have to take into account the spherical shell atmosphere geometry (Thomas and Stamnes, 1998). It is expected that “truth” can be established from *in situ* data obtained from MODIS validation campaigns.

MODIS Airborne Simulator (MAS) observations will be used to optimize cloud detection over snow surfaces. The VIIRS Cloud Mask will be applied over a series of MAS images for which there are varying degrees of snow cover to evaluate and optimize its performance.

## 5.2 PRE-LAUNCH CHARACTERIZATION

The pre-launch plan for the Snow Cover/Depth EDR includes sensitivity studies, analysis of simulated VIIRS data, and verification using MODIS-type data. Observations from AVIRIS, MAS, MODIS, GLI, and NPP will be used in the pre-launch phase to study the error characteristics and optimum techniques for the algorithm. It is expected that MODIS validation data will be of great value. This data is expected to include *in situ* field measurements combined with MODIS observations, MAS underflights, and low level aircraft measurements at spatial resolutions less than 10 meters. Our plan is to use this data in combination with the VIIRS sensor model to produce simulated VIIRS scenes, apply our algorithms to retrieve our EDR products, and compare our results with "truth" derived from *in situ*, aircraft, and MAS data.

## 5.3 VALIDATION

Our pre-launch plan is designed to interface smoothly with post-launch validation activity. We would propose to conduct a post-launch VIIRS validation campaign similar to the MODIS validation activity. In this sense, post-launch validation will already have been simulated by the pre-launch activity. Following launch, we would substitute real VIIRS data for the pre-launch simulated data. We would establish "truth" by the same process as use for pre-launch characterization.

# 6.0 ASSUMPTIONS

The statements and conclusions in this document are subject to the validity of the following assumptions.

1. An effective cloud mask over snow and ice surfaces will be available from the VIIRS Cloud Mask algorithm *[Y2412]*.

2. Surface reflectance brought to standard conditions will be derived from TOA radiances by the Atmospheric Correction over Land algorithm, with errors as specified in the Atmospheric Correction over Land ATBD *[Y2411]*.

3. Pixels subject to large forest canopy errors can be identified and flagged.

4. Non-snow reflectance will be available from an external global database. The creation of this database is a required initialization activity.

# 7.0 REFERENCES

Ackerman, S. *et al.* (1997). Discriminating clear sky from cloud with MODIS. 1997.ATBD MOD-06. *http://eospso.gsfc.nasa.gov/atbd/modistables.html*

Bohren, C.F., and B.R. Barkstrom (1974). Theory of the optical properties of snow. *J. Geophys. Res.*, 79, 4527-4535.

Bromwich, D.H. and R.-Y. Tzeng (1994). Simulation of the modern arctic climate by the NCAR CCM1. *J. Climate***,** 7, 1050-1069.

Carroll, T.R., J.V. Baglio, Jr., J.P. Verdin, and E.W. Holroyd, III (1989). Operational mapping of snow cover in the United States and Canada, using airborne and satellite data. *Proceedings of the 12th Canadian Symposium on Remote Sensing*, V. 3, IGARSS '89, 10-14 July 1989, Vancouver, Canada.

Carroll, T.R., (1990). Operational airborne and satellite snow cover products of the National Operational Hydrologic Remote Sensing Center. *Proceedings of the 47th annual Eastern Snow Conference*, June 7-8, 1990, Bangor, Maine, CRREL Special Report 90-44.

Chang, A.T.C. (1998). AMSR-based SWE retrieval algorithm ATBD. *http://wwwghcc.msfc.nasa.gov/AMSR/snow_ATBD*

Chang, A.T.C. *et al.* (1987). Estimating snowpack parameters in the Colorado River basin. International Association of Hydrological Sciences Publication 166 (Symposium at Vancouver 1987 – *Large Scale Effects of Seasonal Snow Cover*), 343-352.

Crane, R.G. and M.R. Anderson (1984). Satellite discrimination of snow/cloud surfaces. *Intl. J. Remote Sens*., 5(1), 213-223.

Dozier, J. (1984). Snow reflectance from Landsat-4 Thematic Mapper. *IEEE Trans. Geosci. Remote Sens.*, 22(3), 323-328.

Dozier, J. (1989). Spectral signature of alpine snow cover from the Landsat Thematic Mapper. *Remote Sens. Environ.*, 28, 9-22.

Foster, J.L., and A.T.C. Chang (1993). Snow cover. In *Atlas of Satellite Observations Related to Global Change* R.J. Gurney, C.L. Parkinson, and J.L. Foster (eds.), Cambridge University Press, Cambridge, pp. 361-370.

Foster, J.L., A.T.C. Chang, and D.K. Hall (1997). Comparison of snow mass estimates from a prototype passive microwave snow algorithm, a revised algorithm, and a snow depth climatology. *Remote Sens. Environ.*, 62, 132-142.

Grenfell, T.C., D.K. Perovich, and J.A. Ogren (1981). Spectral albedos of an alpine snowpack. *Cold Regions Sci. Technol*., 4, 121-127.

Grody, N.C., and A.N. Basist (1996). Global identification of snow cover using SSM/I instruments. *IEEE Trans. Geosci. Remote Sens.*, 34(1), 237-249.

Hall, D.K., A.Tait, G. Riggs, and V. Salomonson (1998). MODIS: Snow mapping Algorithm and the Sea Ice Mapping Algorithm (Version 4.0). ATBD-MOD-10. *http://eospso.gsfc.nasa.gov/atbd/modistables.html*

Hoffer, R.M. (1978). Biological and physical considerations in applying computer-aided analysis techniques to remote sensor data. In *Remote Sensing: The Quantitative Approach* (P.H. Swain and S.M. Davis, eds.). New York: McGraw-Hill.

Klein,A.G., D.K. Hall, and G.A. Riggs (1998). Improving snow-cover mapping in forests through the use of a canopy reflectance model. *Hydrological Processes*, 12(10-11): 1723-1744.

Matson, M., (1991). NOAA satellite snow cover data. *Palaeogeography, Palaeoclimatology, Palaeoecology*, 90: 213-218.

Matson, M., C.F. Roeplewski, and M.S. Varnadore (1986*). An Atlas of Satellite Derived Northern Hemisphere Snow Cover Frequency*. National Weather Service, Washington, D.C. 75pp.

Nolin, A.W., J. Dozier, and L.A.K. Mertes (1993). Mapping alpine snow using a spectral mixture modeling technique. *Annals of Glaciology* 17, 121-124.

Painter, T.H., D.A. Roberts, R.O. Green, and J. Dozier (1998). The effect of grain size on spectral mixture analysis of snow covered area from AVIRIS data. *Remote Sens. of Environ.,* 65(3): 320-332.

Roberts, D.A., M.Gardner, R. Church, S. Ustin, G. Scheer, and R.O. Green (1998). Mapping Chaparral in the Santa Monica Mountains Using Multiple Endmember Spectral Mixture Models. *Remote Sens. of Environ.,* 65(3): 267-279.

Rosenthal, W.C. (1993). Mapping mountain snow cover at subpixel resolution from the Landsat Thematic Mapper. Master's thesis, Univ. Calif. at Santa Barbara.

Rosenthal, W.C., and J. Dozier (1996). Automated mapping of mountain snow cover at subpixel resolution from the Landsat TM. *Water Resources Res.*, 31(1), 115-130.

Thomas, G., and K. Stamnes (1998). Radiative transfer in the atmosphere and ocean. Textbook, Cambridge Atmospheric and Space Sciences Series.

Vermote, E. (1999). MODIS: Atmospheric Correction Algorithm Spectral Reflectances, ATBD-MOD-08. *http://eospso.gsfc.nasa.gov/atbd/modistables.html*

Warren, S.G. (1982). Optical properties of snow. *Rev. Geophys. Space Phys*., 20(1), 67-89.

Warren, S.G., and W.J.Wiscombe (1980). A model for the spectral albedo of snow. II. Snow containing atmospheric aerosols, *J. Atmos. Sci.*, 37(12), 2734-2745.

Wiscombe, W.J., and S.G. Warren (1980). A model for the spectral albedo of snow,1,pure snow. *J. Atmos. Sci.*, 37(12), 2712-2733.